Hamiltonian aspects of three-wave resonant interactions in gas dynamics

1997 J. Phys. A: Math. Gen. 30 4227

(http://iopscience.iop.org/0305-4470/30/12/013)

J. Phys. A: Math. Gen. **30** (1997) 4227–4257. Printed in the UK PII: S0305-4470(97)76770-2

Hamiltonian aspects of three-wave resonant interactions in gas dynamics*

G M Webb†, A Zakharian†, M Brio‡ and G P Zank§

† Lunar and Planetary Laboratory, University of Arizona, Tucson, AZ 85721, USA
‡ Department of Mathematics, University of Arizona, Tucson, AZ 85721, USA
§ Bartol Research Institute, The University of Delaware, Newark, DE 19716, USA

Received 30 July 1996

Abstract. Equations describing three-wave resonant interactions in adiabatic gas dynamics in one Cartesian space dimension derived by Majda and Rosales are expressed in terms of Lagrangian and Hamiltonian variational principles. The equations consist of two coupled integro-differential Burgers equations for the backward and forward sound waves that are coupled by integral terms that describe the resonant reflection of a sound wave off an entropy wave disturbance to produce a reverse sound wave. Similarity solutions and conservation laws for the equations are derived using symmetry group methods for the special case where the entropy disturbance consists of a periodic saw-tooth profile. The solutions are used to illustrate the interplay between the nonlinearity represented by the Burgers self-wave interaction terms and wave dispersion represented by the three-wave resonant interaction terms. Hamiltonian equations in Fourier (p, t) space are also obtained where p is the Fourier space variable corresponding to the fast phase variable θ of the waves. The latter equations are transformed to normal form in order to isolate the normal modes of the system.

1. Introduction

Majda and Rosales [1] considered weakly nonlinear asymptotic equations for resonantly interacting hyperbolic waves in one Cartesian space dimension. For the case of compressible, adiabatic gas dynamics, Majda and Rosales derived a pair of inviscid Burgers equations (one for the forward sound wave and one for the backward sound wave) coupled through a linear integral operator with a given kernel, dependent on the initial data for the contact discontinuity or entropy wave eigenmode. For the forward sound wave Burgers equation, the linear integral operator describes the resonant reflection of the backward sound wave off the entropy wave to generate a forward sound wave. Similarly, the linear integral operator in the backward sound wave Burgers equation describes the resonant reflection of the forward sound wave off an entropy wave to produce a backward sound wave. Resonant wave interactions in this theory are more liable to be significant for extended periodic or near periodic wavetrains than for isolated pulses, since the resonant interactions are strengthened the longer the period of time over which the waves interact.

Almgren [2] and Joly *et al* [3] considered in more detail the conditions for three-wave resonant interactions, including the case of wave propagation in non-homogeneous or non-uniform media. For the case of a non-uniform background state, high frequency waves initially in resonance typically move out of resonance since the $\boldsymbol{k}$-vector of the waves and

* Contribution 96-11 of the University of Arizona Theoretical Astrophysics Program.

0305-4470/97/124227+31$19.50

the frequency ω evolve according to the ray equations (see also [4] for the case of resonant interactions of internal gravity waves in a stratified shear flow). Joly *et al* [3] carried out a detailed study on resonances, and related the resonance conditions to the geometry of planar webs. Cehelsky and Rosales [5] presented an alternative version of the theory for the case where derivatives are not necessarily bounded and shocks may be present. The latter authors used an equation expansion method similar to the Chapman Enskog method for the Boltzmann equation, rather than a multiple scales method, and incorporated a small modification of the wave phases owing to the presence of multiple waves.

Webb *et al* [6] derived equations describing wave–wave interactions in two-fluid cosmic ray hydrodynamics in a non-uniform background flow. In the gas dynamical limit, and for the case of periodic waves propagating through a uniform background medium the latter equations reduce to the Majda Rosales equations for three-wave resonant interactions in adiabatic gas dynamics. Further developments of the theory are described in [7]. The extension of the theory to resonant interactions in gas dynamics in several space dimensions has been developed by Hunter *et al* [8].

The main aim of this paper is to develop a Hamiltonian formulation of the Majda and Rosales [1] equations describing the three-wave resonant interactions of periodic sound waves and entropy waves in adiabatic gas dynamics propagating through a uniform background medium. In section 2 the model equations obtained by Majda and Rosales [1], and the conditions for three-wave resonant interactions are described. In section 3 Lagrangian and Hamiltonian aspects of the equations are discussed. In particular, we obtain the Hamiltonian form of the equations for some of the lower-order harmonic interaction cases, namely the first and second harmonic interactions, and the first, second and fourth harmonic interactions. In section 4, the Lie symmetries and the conservation laws admitted by a restricted version of the equations applicable for the case of a periodic saw-tooth entropy wave profile are discussed. The symmetries are also used to obtain similarity solutions of the equations. Section 5 considers numerical examples of the similarity solutions, including a discussion on the similarity solutions obtained by Majda *et al* [9]. Section 6 considers the Hamiltonian form of the Majda Rosales equations in (p, t) Fourier space, where p is the Fourier space variable corresponding to the fast phase variable θ of the waves. The latter equations are reduced to normal form in order to isolate the normal modes of the system. Section 7 concludes with a summary and discussion.

2. The model equations

Majda and Rosales [1] considered the resonant interaction of periodic, weakly nonlinear sound waves and the entropy wave in adiabatic gas dynamics in one Cartesian space dimension. The Majda and Rosales equations were derived using weakly nonlinear geometrical optics expansions of the governing equations for high frequency waves.

The basic gas dynamical equations consist of the continuity equation, the momentum equation, the gas entropy equation, plus the adiabatic equation of state relating the gas pressure $p_g = p_g(\rho, S)$ to the gas density ρ and entropy S. Majda and Rosales considered the propagation of weakly nonlinear short wavelength waves about a uniform background state $\rho = \rho_0$, $u = 0$, and $S = S_0$ (u denotes the velocity of the gas along the x-axis), and assumed a perturbation expansion of the form:

$$\psi = \psi^{(0)} + \epsilon\psi^{(1)} + \epsilon^2\psi^{(2)} + \cdots \tag{2.1}$$

where $\psi = (\rho, u, S)$ denotes the state vector of the gas, and ϵ is the perturbation parameter representing the wave amplitude. At lowest order in the perturbation expansion one obtains

the standard eigenvector solutions $\{\boldsymbol{R}_j : j = 1, 2, 3\}$ and eigenvalues $\{\lambda_j : j = 1, 2, 3\}$ of adiabatic gas dynamics, where $\lambda_1 = -a_g$, $\lambda_2 = 0$ and $\lambda_3 = a_g$ are the eigenvalues corresponding to the backward sound wave, the entropy wave and the forward sound wave respectively (here $a_g = (\gamma_g p_g/\rho)^{\frac{1}{2}}$ denotes the gas sound speed, and γ_g is the adiabatic index of the gas).

From the second-order perturbation equations one obtains compatibility conditions on the first-order perturbations by requiring the perturbation expansion is uniform for times $t < \mathrm{O}(1/\epsilon)$ (i.e. it is required that $\epsilon^2\psi^{(2)} < \epsilon\psi^{(1)}$ for times $t < \mathrm{O}(1/\epsilon)$). This leads to the Majda Rosales equations:

$$u_t + u_x + uu_{\theta_3} - \frac{n}{m}\frac{1}{2\pi}\int_0^{2\pi} K(m\theta_3 + n\theta_1, x)v(\theta_1; x, t)\,\mathrm{d}\theta_1 = 0 \tag{2.2}$$

$$v_t - v_x + vv_{\theta_1} + \frac{m}{n}\frac{1}{2\pi}\int_0^{2\pi} K(m\theta_3 + n\theta_1, x)u(\theta_3; x, t)\,\mathrm{d}\theta_3 = 0 \tag{2.3}$$

governing the backward (v) and forward (u) sound wave velocity perturbations. Equations (2.2) and (2.3) correspond to the case of resonant periodic waves in which

$$\theta_j = \frac{k_j x - \omega_j t}{\epsilon} \qquad j = 1, 2, 3 \tag{2.4}$$

correspond to the fast phase variable of the jth wave mode and ω_j and k_j denote the frequencies and wavenumbers of the waves. Equations (2.2) and (2.3) apply to the case of resonant periodic waves and m and n are integers characterizing the resonant interactions. It is assumed in the derivation of equations (2.2) and (2.3) that u and v have period 2π and have zero means in the θ_j. The constraint that u and v have zero means can be lifted, but leads to more complicated equations (see, e.g. Webb *et al* [6]). The period assumed for u and v can be chosen to be any positive constant T, in which case 2π is replaced by T in equations (2.2) and (2.3).

In equations (2.2) and (2.3)

$$u = \frac{\gamma_g + 1}{2}k_3 v_3 \qquad v = \frac{\gamma_g + 1}{2}k_1 v_1 \tag{2.5}$$

correspond to the velocity perturbations v_3 and v_1 associated with the forward and backward sound waves. The kernel

$$K(\theta_2, x) = \frac{k_2}{4}\frac{\partial a_2(\theta_2, x)}{\partial\theta_2} \tag{2.6}$$

represents the derivative of the density perturbation $a_2(\theta_2, x)$ associated with the entropy wave. The velocity perturbations and gas density perturbations in the above equations are normalized to the gas sound speed $a_g = (\gamma_g p_{g0}/\rho_0)^{\frac{1}{2}}$ and density ρ_0 characteristic of the background state.

The integral terms in equations (2.2) and (2.3) represent the resonant interaction of a sound wave with the entropy wave to produce a reverse sound wave, whereas the uu_{θ_3} and vv_{θ_1} terms are the Burgers self-wave interaction terms. Note that there is no separate equation for the entropy wave, since the entropy wave fluctuations are frozen into the background flow. Since $u_0 = 0$, $K(\theta_2, x)$ is completely determined by the initial conditions. The fact that there is no generation of entropy wave disturbances by the three wave interactions is a consequence of the fact that the entropy is a Riemann invariant of the gas dynamical equations (Majda and Rosales, [1]).

2.1. Resonance conditions

For resonant 2π-periodic waves in the θ_j, the frequencies ω_j and wavenumbers k_j satisfy the resonance conditions:

$$k_2 = nk_1 + mk_3 \qquad \omega_2 = n\omega_1 + m\omega_3 \tag{2.7}$$

where m and n are integers (see, e.g. Anile *et al* [7]). Since the velocity perturbations are normalized to the gas sound speed, the dispersion equations for the waves are:

$$\omega_1 = -k_1 \qquad \omega_2 = 0 \qquad \omega_3 = k_3 \tag{2.8}$$

corresponding to the backward sound wave, the entropy wave and the forward sound wave respectively. Equations (2.7) and (2.8) imply that

$$\frac{k_2}{2k_1} = n \qquad \frac{k_2}{2k_3} = m \tag{2.9}$$

for resonant-wave interactions. In terms of the wavelength of the waves $\{\ell_j\}$, equations (2.9) imply

$$\ell_1 = 2\ell_2|n| \qquad \ell_3 = 2\ell_2|m| \tag{2.10}$$

so that the wavelengths of the sound waves are integral multiples of the wavelength of the entropy wave for resonant waves.

2.2. The analogue of the Manley–Rowe relations

First note that equations (2.2) and (2.3) may be written in the form:

$$u_t + u_x + uu_\theta - \frac{n}{m}\frac{1}{2\pi}\int_0^{2\pi} K(m\theta + n\xi, x)v(\xi; x, t)\,\mathrm{d}\xi = 0 \tag{2.11}$$

$$v_t - v_x + vv_\theta + \frac{m}{n}\frac{1}{2\pi}\int_0^{2\pi} K(m\xi + n\theta, x)u(\xi; x, t)\,\mathrm{d}\xi = 0 \tag{2.12}$$

where the variable θ in equation (2.11) refers to the phase of the forward sound wave, whereas in equation (2.12) θ refers to the phase of the backward sound wave. It is of interest to note that equations (2.11) and (2.12) may be written in the conservative form:

$$u_t + u_x + \frac{\partial}{\partial\theta}\left(\frac{u^2}{2} - \frac{n}{m^2}\frac{1}{2\pi}\int_0^{2\pi} R(m\theta + n\xi, x)v(\xi; x, t)\,\mathrm{d}\xi\right) = 0 \tag{2.13}$$

$$v_t - v_x + \frac{\partial}{\partial\theta}\left(\frac{v^2}{2} + \frac{m}{n^2}\frac{1}{2\pi}\int_0^{2\pi} R(m\xi + n\theta, x)u(\xi; x, t)\,\mathrm{d}\xi\right) = 0 \tag{2.14}$$

where the equations:

$$R(\theta_2, x) = \frac{k_2}{4}a_2(\theta_2, x) \qquad K(\theta_2, x) = \frac{\partial R(\theta_2, x)}{\partial\theta_2} \tag{2.15}$$

relate the kernel $R(\theta_2, x)$ to the entropy wave density perturbation $a_2(\theta_2, x)$ and to the kernel $K(\theta_2, x)$.

Multiplying equation (2.11) by m^2u and adding equation (2.12) multiplied by n^2v and integrating with respect to θ from $\theta = 0$ to $\theta = 2\pi$ yields the equation:

$$\frac{\partial}{\partial t}\left(\int_0^{2\pi}\frac{m^2u^2}{2} + \frac{n^2v^2}{2}\,\mathrm{d}\theta\right) + \frac{\partial}{\partial x}\left(\int_0^{2\pi}\frac{m^2u^2}{2} - \frac{n^2v^2}{2}\,\mathrm{d}\theta\right) + \sum_s\left[\frac{m^2u^3}{3} + \frac{n^2v^3}{3}\right]_{\theta_{s+}}^{\theta_{s-}} = 0 \tag{2.16}$$

where the sum over s corresponds to shocks at the points $\theta = \theta_s$ that possibly occur in the θ range: $0 < \theta < 2\pi$. Equation (2.16) is the analogue of the Manley–Rowe relations for three-wave resonant interactions of dispersive waves (see, e.g. Anile *et al* [7]).

2.3. Special forms of the equations

Below we discuss special forms of the equations which we consider in more detail in the following sections. In particular we discuss the form of the equations for the case of a periodic saw-tooth entropy wave profile in θ_2 which allows the evaluation of the integrals in the three-wave resonant interaction terms in equations (2.11) and (2.12).

2.3.1. Case (a): $m = 1$ and $n = -1$. Equations (2.11) and (2.12) in this case reduce to:

$$u_t + u_x + uu_\theta + \frac{1}{2\pi}\int_0^{2\pi} K(\theta - \xi, x)v(\xi; x, t)\,\mathrm{d}\xi = 0 \tag{2.17}$$

$$v_t - v_x + vv_\theta - \frac{1}{2\pi}\int_0^{2\pi} K(\xi - \theta, x)u(\xi; x, t)\,\mathrm{d}\xi = 0. \tag{2.18}$$

Pego [10], Majda *et al* [9] and Hunter [11] considered analytical and numerical solutions of equations (2.17) and (2.18) that were independent of the long space variable x. For the model equations (2.17) and (2.18) the wavelengths of the sound waves are twice that of the entropy wave (see equations (2.10)). Pego [10] derived periodic, smooth analytic solutions of equations (2.17) and (2.18) for the case of a periodic kernel $K(\theta) = \sin\theta$ (see also the discussion by Anile *et al* [7]) in which the resonant interactions counteract the tendency of the solutions to form shocks due to the nonlinear Burgers terms.

For the case of a periodic saw-tooth entropy profile:

$$R(\theta) = \alpha(\theta - \pi) \qquad \text{for } 0 < \theta < 2\pi \tag{2.19}$$

(α is a constant) periodically extended with a period of 2π in θ, the kernel $K(\theta)$ has the form:

$$K(\theta) = \alpha\left\{1 - 2\pi \sum_{n=-\infty}^{\infty} \delta[\theta - 2n\pi]\right\}. \tag{2.20}$$

Substituting kernel (2.20) into equations (2.17) and (2.18) yields the coupled Burgers equations:

$$u_t + u_x + uu_\theta - \alpha v(\theta; x, t) = 0 \tag{2.21}$$

$$v_t - v_x + vv_\theta + \alpha u(\theta; x, t) = 0 \tag{2.22}$$

governing the resonant interaction of the sound waves. The relevant solutions of equations (2.21) and (2.22) must have zero means, and be periodic in θ.

2.3.2. Case (b): $m = 1$ and $n = 1$. In this case the resonant interaction equations (2.11) and (2.12) reduce to:

$$u_t + u_x + uu_\theta - \frac{1}{2\pi}\int_0^{2\pi} K(\theta + \xi, x)v(\xi; x, t)\,\mathrm{d}\xi = 0 \tag{2.23}$$

$$v_t - v_x + vv_\theta + \frac{1}{2\pi}\int_0^{2\pi} K(\theta + \xi, x)u(\xi; x, t)\,\mathrm{d}\xi = 0. \tag{2.24}$$

For the saw-tooth entropy wave profile (2.19), these equations reduce to:

$$u_t + u_x + uu_\theta + \alpha v(-\theta; x, t) = 0 \tag{2.25}$$

$$v_t - v_x + vv_\theta - \alpha u(-\theta; x, t) = 0. \tag{2.26}$$

The interesting point to note in this case is that the coupled Burgers equations (2.25) and (2.26) are now non-local equations, whereas the Burgers equations (2.21) and (2.22) for the case (*a*) $m = 1$ and $n = -1$ are local equations.

2.3.3. Case (c) $m = 1$ and $n = -2$. For the saw-tooth entropy wave profile the kernel $K(\theta)$ is given by equation (2.20), and the Burgers equations (2.11) and (2.12) reduce to:

$$u_t + u_x + uu_\theta - \alpha[v(\tfrac{1}{2}\theta; x, t) + v(\tfrac{1}{2}\theta + \pi; x, t)] = 0 \tag{2.27}$$

$$v_t - v_x + vv_\theta + \tfrac{1}{2}\alpha u(2\theta; x, t) = 0. \tag{2.28}$$

Again, we obtain non-local coupled Burgers equations for u and v. In this case, the resonance conditions (2.9) yield

$$k_1 = -\frac{k_2}{4} \qquad k_3 = \frac{k_2}{2} \tag{2.29}$$

so that the backward sound wave has a wavelength of $\ell_1 = 4\ell_2$, and the forward sound wave has a wavelength of $\ell_3 = 2\ell_2$ where ℓ_2 is the wavelength of the entropy wave.

3. Variational formulations

In this section we obtain Lagrangian and Hamiltonian variational principles for the Majda and Rosales equations (2.11) and (2.12). We illustrate some of the complications that can arise for different m and n by considering the examples (i) $m = 1$ and $n = -1$ and (ii) $m = 1$ and $n = -2$.

3.1. Case $m = 1$ and $n = -1$

The basic equations of interest are equations (2.17) and (2.18), namely

$$u_t + u_x + uu_\theta + \hat{K}[v] = 0 \tag{3.1}$$

$$v_t - v_x + vv_\theta - \hat{K}^\dagger[u] = 0 \tag{3.2}$$

where the integral operators $\hat{K}$ and $\hat{K}^\dagger$ are defined by the equations:

$$\hat{K}[v] = \frac{1}{2\pi}\int_0^{2\pi} K(\theta - \xi, x)v(\xi; x, t)\,\mathrm{d}\xi \tag{3.3}$$

$$\hat{K}^\dagger[u] = \frac{1}{2\pi}\int_0^{2\pi} K(\xi - \theta, x)u(\xi; x, t)\,\mathrm{d}\xi. \tag{3.4}$$

In equations (3.1)–(3.4) $\hat{K}^\dagger$ is the adjoint of the operator $\hat{K}$ with respect to the standard inner product

$$\langle f, g\rangle = \int_0^{2\pi} f(\xi)g(\xi)\,\mathrm{d}\xi. \tag{3.5}$$

To obtain a Lagrangian variational principle for these equations, first introduce potential variables $U(\theta; x, t)$ and $V(\theta; x, t)$ such that

$$u = U_\theta \qquad v = V_\theta. \tag{3.6}$$

By noting that the operators $\hat{K}$ and $\hat{K}^\dagger$ commute with $D_\theta \equiv \partial/\partial\theta$, i.e.

$$D_\theta(\hat{K}[V]) = \hat{K}[D_\theta V] \qquad D_\theta(\hat{K}^\dagger[U]) = \hat{K}^\dagger[D_\theta U] \tag{3.7}$$

one finds that equations (3.1) and (3.2) may be written in the potential form:

$$D_\theta(U_t + U_x + \tfrac{1}{2}U_\theta^2 + \hat{K}[V]) = 0 \tag{3.8}$$

$$D_\theta(V_t - V_x + \tfrac{1}{2}V_\theta^2 - \hat{K}^\dagger[U]) = 0. \tag{3.9}$$

Equations (3.8) and (3.9) may be obtained from the variational principle of extremizing the Lagrangian variational functional:

$$L = \int_{-\infty}^{\infty} \mathrm{d}t \int_{-\infty}^{\infty} \mathrm{d}x \int_{0}^{2\pi} \mathrm{d}\theta\, \mathcal{L} \tag{3.10}$$

where

$$\mathcal{L} = -\tfrac{1}{2}(U_\theta U_t + V_\theta V_t) - \tfrac{1}{2}(U_x U_\theta - V_x V_\theta) - \tfrac{1}{6}(U_\theta^3 + V_\theta^3) + \tfrac{1}{2}(\hat{K}^\dagger[U]V_\theta - \hat{K}[V]U_\theta) \tag{3.11}$$

is the Lagrangian density.

Equations (3.1) and (3.2) may also be written in the Hamiltonian form:

$$u_t = D_\theta\left(\frac{\delta H}{\delta u}\right) \qquad v_t = D_\theta\left(\frac{\delta H}{\delta v}\right) \tag{3.12}$$

where the Hamiltonian functional has the form:

$$H = \int_{-\infty}^{\infty} \mathrm{d}x \int_{0}^{2\pi} \mathrm{d}\theta\, \mathcal{H} \tag{3.13}$$

$$\mathcal{H} = -\tfrac{1}{6}(u^3 + v^3) - \tfrac{1}{2}(u D_\theta^{-1} u_x - v D_\theta^{-1} v_x) - \tfrac{1}{2}\{u\hat{K}[D_\theta^{-1}v] - v\hat{K}^\dagger[D_\theta^{-1}u]\}$$

and $D_\theta^{-1} f \equiv \int^\theta \mathrm{d}\theta\, f(\theta)$. In equations (3.12) D_θ is the symplectic operator (e.g. [12]). Alternatively, using the Poisson bracket for functionals F and G:

$$\{F, G\} = \int_0^{2\pi} \mathrm{d}\theta\, \frac{\delta F}{\delta u^\alpha} D_\theta\left(\frac{\delta G}{\delta u^\alpha}\right) \tag{3.14}$$

where $(u^1, u^2) \equiv (u, v)$ equations (3.12) may be written in the form:

$$u_t = \{u, H\} \qquad v_t = \{v, H\}. \tag{3.15}$$

For the case of a saw-tooth entropy wave profile (2.19), the Lagrangian density $\mathcal{L}$ in equation (3.11) takes the form:

$$\mathcal{L}_\alpha = -\tfrac{1}{2}(U_\theta U_t + V_\theta V_t) - \tfrac{1}{2}(U_x U_\theta - V_x V_\theta) - \tfrac{1}{6}(U_\theta^3 + V_\theta^3) - \tfrac{1}{2}\alpha(U V_\theta - V U_\theta) \tag{3.16}$$

and a similar result applies for the Hamiltonian density in equations (3.13).

3.2. Case $m = 1$ and $n = -2$

In this section we show the kind of complications that arise for cases where $m \neq 1$ and $n \neq -1$. The examples of saw-tooth entropy profiles discussed in equations (2.25) and (2.26) for $m = 1$, $n = 1$ and in equations (2.27) and (2.28) for the case $m = 1$ and $n = -2$ lead to non-local coupled Burgers equations for the backward and forward sound waves.

Equations (2.11) and (2.12) for the case $m = 1$ and $n = -2$ reduce to:

$$u_t + u_x + u u_\theta + \frac{1}{\pi}\int_0^{2\pi} K(\theta - 2\xi, x) v(\xi; x, t)\, \mathrm{d}\xi = 0 \tag{3.17}$$

$$v_t - v_x + v v_\theta - \frac{1}{4\pi}\int_0^{2\pi} K(\xi - 2\theta, x) u(\xi; x, t)\, \mathrm{d}\xi = 0. \tag{3.18}$$

For the case of a saw-tooth entropy wave profile (2.19), equations (3.17) and (3.18) reduce to equations (2.27) and (2.28), in which $u(\theta; x, t)$, $u(2\theta; x, t)$, $v(\theta; x, t)$, $v(\frac{1}{2}\theta; x, t)$ and $v(\frac{1}{2}\theta + \pi; x, t)$ play a role. Equation (3.17) may be written in the form:

$$u_t + u_x + u u_\theta + \frac{1}{2\pi}\int_0^{2\pi} K(\theta - \eta; x, t)[v(\tfrac{1}{2}\eta; x, t) + v(\tfrac{1}{2}\eta + \pi; x, t)]\, \mathrm{d}\eta = 0. \tag{3.19}$$

Hence $v(\frac{1}{2}\eta; x, t)$ and $v(\frac{1}{2}\eta + \pi; x, t)$ also play an important role in equations (3.17) and (3.18).

Motivated by the above observations we introduce new variables:

$$z_1(\theta; x, t) = 2^{\frac{1}{2}} v(\tfrac{1}{2}\theta; x, t) \qquad z_2(\theta; x, t) = 2^{\frac{1}{2}} v(\tfrac{1}{2}\theta + \pi; x, t) \tag{3.20}$$

where $0 \leqslant \theta \leqslant 2\pi$. Note that $v(\theta; x, t)$ can be reconstructed from $z_1(\theta; x, t)$ and $z_2(\theta; x, t)$. The functions u, z_1 and z_2 satisfy the coupled equations:

$$\begin{aligned} &u_t + u_x + uu_\theta + 2^{-\frac{1}{2}} \hat{K}[z_1 + z_2] = 0 \\ &z_{1t} - z_{1x} + 2^{\frac{1}{2}} z_1 z_{1\theta} - 2^{-\frac{1}{2}} \hat{K}^\dagger[u] = 0 \\ &z_{2t} - z_{2x} + 2^{\frac{1}{2}} z_2 z_{2\theta} - 2^{-\frac{1}{2}} \hat{K}^\dagger[u] = 0. \end{aligned} \tag{3.21}$$

Note that z_1 and z_2 satisfy the same partial differential equation. One possible solution of these equations is $z_1 = z_2$, although this will not generally be the case, unless $v(\theta; x, t)$ has a period of π in θ. If $v(\theta; x, t)$ does not have a shock at $\theta = \pi$, then $z_1(2\pi; x, t) = z_2(0; x, t)$, and higher-order derivatives of v would match at $\theta = \pi$. Using the notation:

$$\psi = (u, z_1, z_2)^T \qquad \psi^2 = (u^2, z_1^2, z_2^2)^T \tag{3.22}$$

(the superscript T denotes the transpose), equations (3.21) may be written in the matrix form:

$$\frac{\partial \psi}{\partial t} + \mathbf{A}\cdot\frac{\partial \psi}{\partial x} + \frac{1}{2} D_\theta(\mathbf{B}\cdot\psi^2) + \tilde{\mathbf{K}}\cdot\psi = 0 \tag{3.23}$$

where the matrices $\mathbf{A}$ and $\mathbf{B}$ are given by

$$\begin{aligned} \mathbf{A} &= \begin{pmatrix} 1 & 0 & 0 \\ 0 & -1 & 0 \\ 0 & 0 & -1 \end{pmatrix} \\ \mathbf{B} &= \begin{pmatrix} 1 & 0 & 0 \\ 0 & 2^{\frac{1}{2}} & 0 \\ 0 & 0 & 2^{\frac{1}{2}} \end{pmatrix} \end{aligned} \tag{3.24}$$

and the matrix operator $\tilde{\mathbf{K}}$ has the form:

$$\tilde{\mathbf{K}} = \frac{1}{2^{\frac{1}{2}}} \begin{pmatrix} 0 & \hat{K} & \hat{K} \\ -\hat{K}^\dagger & 0 & 0 \\ -\hat{K}^\dagger & 0 & 0 \end{pmatrix}. \tag{3.25}$$

The operators $\hat{K}$ and $\hat{K}^\dagger$ are defined in equations (3.3) and (3.4) where $\hat{K}^\dagger$ is the adjoint of $\hat{K}$. The matrix operator in equation (3.25) is skew adjoint (i.e. $\tilde{\mathbf{K}}^\dagger = -\tilde{\mathbf{K}}^T$).

Introducing the potential variables:

$$\Psi = (U, Z_1, Z_2)^T \qquad \psi = \Psi_\theta \equiv (u, z_1, z_2)^T \tag{3.26}$$

equations (3.23) may be written in the potential form:

$$D_\theta(\Psi_t + \mathbf{A}\cdot\Psi_x + \tfrac{1}{2}\mathbf{B}\cdot\Psi_\theta^2 + \tilde{\mathbf{K}}\cdot\Psi) = 0. \tag{3.27}$$

In the derivation of equation (3.27) we use the fact that the operators $\hat{K}$ and $\hat{K}^\dagger$ commute with D_θ (see equations (3.7)). The notation:

$$\Psi_\theta^2 \equiv (U_\theta^2, Z_{1\theta}^2, Z_{2\theta}^2)^T \tag{3.28}$$

is used in equation (3.27).

Equations (3.27) may be obtained by extremizing the variational functional

$$L = \int_{-\infty}^{\infty} \mathrm{d}t \int_{-\infty}^{\infty} \mathrm{d}x \int_{0}^{2\pi} \mathrm{d}\theta \, \mathcal{L} \tag{3.29}$$

where

$$\mathcal{L} = -\tfrac{1}{2}\Psi_\theta^T \cdot \Psi_t - \tfrac{1}{2}\Psi_\theta^T \cdot \mathbf{A} \cdot \Psi_x - \tfrac{1}{2}\Psi_\theta^T \cdot \tilde{\mathbf{K}} \cdot \Psi - \tfrac{1}{6}(\Psi_\theta^2)^T \cdot \mathbf{B} \cdot \Psi_\theta. \tag{3.30}$$

Alternatively in component form:

$$\begin{aligned}\mathcal{L} = {} & -\tfrac{1}{2}(U_\theta U_t + Z_{1\theta} Z_{1t} + Z_{2\theta} Z_{2t}) - \tfrac{1}{2}(U_\theta U_x - Z_{1\theta} Z_{1x} - Z_{2\theta} Z_{2x}) \\ & -2^{-\frac{3}{2}}\{U_\theta \hat{K}[Z_1 + Z_2] - (Z_{1\theta} + Z_{2\theta})\hat{K}^\dagger[U]\} - \tfrac{1}{6}[U_\theta^3 + 2^{\frac{1}{2}}(Z_{1\theta}^3 + Z_{2\theta}^3)].\end{aligned} \tag{3.31}$$

The variational principle (3.29) yields equations (3.21). Note, however that further constraints may need to be applied to the variational functional (3.29) if $v(\theta; x, t)$ is to be smooth at $\theta = \pi$.

Equations (3.23) can also be written in the Hamiltonian form:

$$\psi_t = D_\theta \left(\frac{\delta H}{\delta \psi} \right) \tag{3.32}$$

where the Hamiltonian functional is given by:

$$H = \int_{-\infty}^{\infty} \mathrm{d}x \int_{0}^{2\pi} \mathrm{d}\theta \, [-\tfrac{1}{2}\Psi_\theta^T \cdot \mathbf{A} \cdot \Psi_x - \tfrac{1}{2}\Psi_\theta^T \cdot \tilde{\mathbf{K}} \cdot \Psi - \tfrac{1}{6}(\Psi_\theta^2)^T \cdot \mathbf{B} \cdot \Psi_\theta]. \tag{3.33}$$

The above development for the case $m = 1$, and $n = -2$ shows that for $m \neq 1$, $n \neq -1$, it is necessary in general to introduce new variables to reduce the equations to Hamiltonian form. Clearly the above analysis can be generalized for more general m and n.

4. Symmetries and conservation laws

In this section we discuss the symmetries and conservation laws for the coupled Burgers equations (2.21) and (2.22) governing the resonant interaction of the backward and forward sound waves for the case of a saw-tooth entropy wave profile described by equations (2.19) and (2.20). The symmetries are also used to derive similarity solutions of the equations. We restrict our attention to solutions which are independent of the long space variable x. Thus, the equations of interest are:

$$u_t + u u_\theta - \alpha v(\theta, t) = 0 \tag{4.1}$$

$$v_t + v v_\theta + \alpha u(\theta, t) = 0 \tag{4.2}$$

where α is a constant.

Equations (4.1) and (4.2) may be obtained from the variational principle (see equations (3.10)–(3.16)) of extremizing the functional:

$$\begin{aligned} L &= \int_{-\infty}^{\infty} \mathrm{d}t \int_{0}^{2\pi} \mathrm{d}\theta \, \mathcal{L}_\alpha \\ \mathcal{L}_\alpha &= -\tfrac{1}{2}(U_\theta U_t + V_\theta V_t) - \tfrac{1}{6}(U_\theta^3 + V_\theta^3) - \tfrac{1}{2}\alpha(U V_\theta - V U_\theta) \end{aligned} \tag{4.3}$$

where $u = U_\theta$ and $v = V_\theta$. The potential form of equations (4.1) and (4.2) are also of interest are, namely:

$$U_t + \tfrac{1}{2}U_\theta^2 - \alpha V = 0 \tag{4.4}$$

$$V_t + \tfrac{1}{2}V_\theta^2 + \alpha U = 0. \tag{4.5}$$

The Lie point symmetries admitted by equations (4.1) and (4.2), and equations (4.4) and (4.5) are discussed in section 4.1. In section 4.2 conservation laws for the equations are obtained by using the variational formulation (4.3) of the equations in conjunction with Noether's theorem. Section 4.3 considers similarity solutions of the equations and their relation to analytic solutions obtained by Majda *et al* [9].

4.1. Lie point symmetries

Equations (4.1) and (4.2) admit infinitesimal Lie point symmetries of the form:

$$t' = t + \epsilon\xi^t \qquad \theta' = \theta + \epsilon\xi^\theta \qquad u' = u + \epsilon\eta^u \qquad v' = v + \epsilon\eta^v \tag{4.6}$$

where the infinitesimal generators $(\xi^t, \xi^\theta, \eta^u, \eta^v)$ are given by:

$$\xi^t = a_1 \qquad \xi^\theta = a_2 + a_3\theta \qquad \eta^u = a_3 u \qquad \eta^v = a_3 v \tag{4.7}$$

and a_1, a_2 and a_3 are constants. The corresponding point Lie algebra has the general isovector

$$X = \xi^t\frac{\partial}{\partial t} + \xi^\theta\frac{\partial}{\partial\theta} + \eta^u\frac{\partial}{\partial u} + \eta^v\frac{\partial}{\partial v} \equiv a_1X_1 + a_2X_2 + a_3X_3 \tag{4.8}$$

where

$$\begin{aligned} X_1 &= \frac{\partial}{\partial t} \\ X_2 &= \frac{\partial}{\partial\theta} \\ X_3 &= \theta\frac{\partial}{\partial\theta} + u\frac{\partial}{\partial u} + v\frac{\partial}{\partial v} \end{aligned} \tag{4.9}$$

are the basis elements of the Lie algebra. The operators X_1, X_2 and X_3 correspond respectively to the time translation symmetry, θ-translation symmetry and a 'stretch' symmetry of equations (4.1) and (4.2).

Using results (4.7)–(4.9) one can show that the potential equations (4.4) and (4.5) admit the Lie symmetry operators:

$$\begin{aligned} Y_1 &= \frac{\partial}{\partial t} \\ Y_2 &= \frac{\partial}{\partial\theta} \\ Y_3 &= \theta\frac{\partial}{\partial\theta} + 2U\frac{\partial}{\partial U} + 2V\frac{\partial}{\partial V} \\ Y_4 \equiv Y_\delta &= \sin(\alpha t + \delta)\frac{\partial}{\partial U} + \cos(\alpha t + \delta)\frac{\partial}{\partial V}. \end{aligned} \tag{4.10}$$

The symmetry operators Y_1, Y_2 and Y_3 in equations (4.10) correspond to the symmetry operators $\{X_1, X_2, X_3\}$ of equations (4.9) associated with equations (4.1) and (4.2). The operator Y_4 in equations (4.10) corresponds to the fact that the potential equations (4.4) and (4.5) remain invariant under the transformations:

$$U' = U + \epsilon\sin(\alpha t + \delta) \qquad V' = V + \epsilon\cos(\alpha t + \delta) \tag{4.11}$$

which are gauge symmetries.

4.2. Conservation laws

Using the symmetries (4.10) of the potential equations (4.4) and (4.5), the variational principle (4.3) and applying Noether's theorem (e.g. Bluman and Kumei [13], Olver [14]) leads to four conservation laws associated with equations (4.1) and (4.2) and (4.4) and (4.5) of the form:

$$D_t E_j + D_\theta F_j = 0 \qquad j = 1(1)4 \tag{4.12}$$

where $D_t \equiv \partial/\partial t$ and $D_\theta \equiv \partial/\partial\theta$. The conserved densities $\{E_j\}$ and fluxes $\{F_j\}$ associated with each of the symmetries are listed below:

$$\begin{aligned} E_1 &= -\tfrac{1}{6}(u^3+v^3) - \tfrac{1}{2}\alpha(Uv - Vu) \\ F_1 &= -\tfrac{1}{8}(u^4+v^4) + \tfrac{1}{4}\alpha(Vu^2 - Uv^2) \end{aligned} \tag{4.13}$$

$$\begin{aligned} E_2 &= \tfrac{1}{2}(u^2+v^2) \\ F_2 &= \tfrac{1}{3}(u^3+v^3) \end{aligned} \tag{4.14}$$

$$\begin{aligned} E_3 &= \tfrac{1}{2}(\theta u^2 + \theta v^2) - (Uu + Vv) + \tfrac{1}{2}D_\theta^{-1}(u^2+v^2) \\ F_3 &= \tfrac{1}{3}\theta(u^3+v^3) - \tfrac{1}{2}(Uu^2 + Vv^2) \end{aligned} \tag{4.15}$$

$$\begin{aligned} E_4 &= u\sin(\alpha t+\delta) + v\cos(\alpha t+\delta) \\ F_4 &= \tfrac{1}{2}[u^2\sin(\alpha t+\delta) + v^2\cos(\alpha t+\delta)]. \end{aligned} \tag{4.16}$$

The conserved density E_1 associated with time translation invariance in equations (4.13) corresponds to the Hamiltonian density, i.e. equations (4.1) and (4.2) may be written in the Hamiltonian form (3.12) where

$$H = \int_0^{2\pi} \mathrm{d}\theta\, E_1 \equiv \int_0^{2\pi} \mathrm{d}\theta\, [-\tfrac{1}{6}(u^3+v^3) - \tfrac{1}{2}\alpha(Uv - Vu)] \tag{4.17}$$

is the Hamiltonian functional.

The conservation law associated with θ-translation invariance (equations (4.14)) corresponds to the Manley–Rowe relations (2.16) discussed in section 2. The conservation law associated with the stretch symmetry Y_3 (equations (4.10) and (4.15)) is the least obvious law. The conservation law (4.16) associated with Y_4 might have been expected from the fact that the linearized version of equations (4.1) and (4.2) admit the trigonometric solutions:

$$u = \sin(\alpha t+\delta) \qquad v = \cos(\alpha t+\delta). \tag{4.18}$$

4.3. Similarity solutions

Classical similarity solutions of equations (4.1) and (4.2) may be obtained by first integrating the group trajectories:

$$\frac{\mathrm{d}t}{\xi^t} = \frac{\mathrm{d}\theta}{\xi^\theta} = \frac{\mathrm{d}u}{\eta^u} = \frac{\mathrm{d}v}{\eta^v} \tag{4.19}$$

to obtain the group invariants (see, e.g. [13]). In the present case the infinitesimal generators of the point Lie group are given by equations (4.7), so that equations (4.19) reduce to:

$$\frac{\mathrm{d}t}{a_1} = \frac{\mathrm{d}\theta}{a_2 + a_3\theta} = \frac{\mathrm{d}u}{a_3 u} = \frac{\mathrm{d}v}{a_3 v}. \tag{4.20}$$

Integrating the group trajectories (4.20), assuming $a_1 \neq 0$ and $a_3 \neq 0$ yields the group invariants:

$$J_1 = \ln|\theta - \theta_0| - \mu t \qquad J_2 = \frac{u}{\theta - \theta_0} \qquad J_3 = \frac{v}{\theta - \theta_0} \tag{4.21}$$

where

$$\mu = \frac{a_3}{a_1} \qquad \theta_0 = -\frac{a_2}{a_3}. \tag{4.22}$$

From equations (4.21) and (4.22), it follows that equations (4.1) and (4.2) possess similarity solutions of the form:

$$u = (\theta - \theta_0) f(\eta) \qquad v = (\theta - \theta_0) g(\eta) \tag{4.23}$$

where

$$\eta = \ln|\theta - \theta_0| - \mu t \tag{4.24}$$

is the similarity variable. Substituting the solution ansatz (4.23) and (4.24) into equations (4.1) and (4.2) yields the ordinary differential equations:

$$(f - \mu) f'(\eta) = -(f^2 - \alpha g) \qquad (g - \mu) g'(\eta) = -(g^2 + \alpha f). \tag{4.25}$$

Since equations (4.25) do not depend explicitly on η, the equations may be combined to yield a single ordinary differential equation

$$\frac{\mathrm{d}f}{\mathrm{d}g} = \frac{(f^2 - \alpha g)(g - \mu)}{(g^2 + \alpha f)(f - \mu)} \tag{4.26}$$

in the (f, g) phase plane. It is of interest to note that equation (4.26) is an example of Darboux's equation (e.g. Ince [15, p 29]; Goursat [16, p 29]), i.e. equation (4.26) may be written in the form:

$$\frac{\mathrm{d}f}{\mathrm{d}g} = \frac{Nf - M}{Ng - L} \tag{4.27}$$

where

$$\begin{aligned} M &= \mu f^2 + \alpha g^2 - \mu\alpha g \\ N &= fg \\ L &= \mu g^2 - \alpha f^2 + \mu\alpha f. \end{aligned} \tag{4.28}$$

The general theory of Darboux's equation is described in [15, 16], where further reference to the original work of Darboux may be found.

The general character of the solutions for equations (4.25) and (4.26) may be deduced from an analysis of the critical points of equation (4.26) in the (f, g) phase plane. This is carried out in section 5. For general α and μ, we have not been able to obtain an analytic integral of equation (4.26). However, in the special cases (*a*) $a_3 \to 0$ ($|\theta_0| \to \infty$, $\mu \to 0$) and (*b*) $a_1 \to 0$ ($\mu \to \infty$) Majda *et al* [9] obtained first integrals. The Lagrangian and Hamiltonian structure associated with these solutions are discussed below.

4.3.1. Special solutions.

Case (a): $a_3 = 0$. The similarity solutions for $a_3 = 0$ may be obtained from equations (4.22)–(4.25) by a suitable rescaling of the variables. However, it is simpler just to re-integrate the group trajectories (4.20) with $a_3 = 0$, to obtain the travelling wave similarity solutions:

$$u = u(\eta) \qquad v = v(\eta) \tag{4.29}$$

where the equations:

$$\eta = \theta - \lambda t \qquad \lambda = \frac{a_2}{a_1} \tag{4.30}$$

define the similarity variable.

Substitution of the solution ansatz (4.29) and (4.30) into equations (4.1) and (4.2) yields the equations:

$$(u-\lambda)u'(\eta)=\alpha v \qquad (v-\lambda)v'(\eta)=-\alpha u. \tag{4.31}$$

Equations (4.31) may be combined to yield the differential equation

$$\frac{\mathrm{d}u}{\mathrm{d}v}=-\frac{v(v-\lambda)}{u(u-\lambda)} \tag{4.32}$$

with integral

$$H=\tfrac{1}{3}(u^3+v^3)-\tfrac{1}{2}\lambda(u^2+v^2) \tag{4.33}$$

where H is the integration constant. Integral (4.33) was obtained by Majda *et al* [9]. Below it is shown that H is the Hamiltonian for equations (4.31).

Introducing the canonical variables:

$$q_1=\frac{a(u-\lambda)^2}{2\alpha^{\frac{1}{2}}} \qquad p_1=\frac{(v-\lambda)^2}{2a\alpha^{\frac{1}{2}}} \tag{4.34}$$

(where a is an arbitrary constant), equations (4.31) may be written in the Hamiltonian form:

$$\begin{aligned}\frac{\mathrm{d}q_1}{\mathrm{d}\eta}&=\frac{\partial H}{\partial p_1}\equiv a\alpha^{\frac{1}{2}}v\\ \frac{\mathrm{d}p_1}{\mathrm{d}\eta}&=-\frac{\partial H}{\partial q_1}\equiv-\frac{\alpha^{\frac{1}{2}}u}{a}.\end{aligned} \tag{4.35}$$

Using results (4.33)–(4.35) it follows that equations (4.31) may also be obtained by extremizing the variational functional

$$L=\int\left(\frac{(v-\lambda)^2(u-\lambda)}{2\alpha}u'(\eta)-\frac{u^3+v^3}{3}+\frac{\lambda(u^2+v^2)}{2}\right)\mathrm{d}\eta. \tag{4.36}$$

Alternative canonical variables to $\{q_1, p_1\}$ can be chosen. It is straightforward to verify that

$$q_2=u \qquad p_2=\frac{(v-\lambda)^2(u-\lambda)}{2\alpha} \tag{4.37}$$

are also canonical variables for equations (4.31) with Hamiltonian (4.33).

Case (b): $a_1=0$. Integrating the group trajectories (4.20) for this case yields similarity solutions of the form:

$$u=(\theta-\theta_0)f(t) \qquad v=(\theta-\theta_0)g(t) \tag{4.38}$$

where $\eta\equiv t$ is the similarity variable. Substitution of the solution ansatz (4.38) into equations (4.1) and (4.2) yields the ordinary differential equations:

$$f'(t)=-(f^2-\alpha g) \qquad g'(t)=-(g^2+\alpha f). \tag{4.39}$$

Equations (4.39) may be combined to yield the differential equation

$$\frac{\mathrm{d}f}{\mathrm{d}g}=\frac{f^2-\alpha g}{g^2+\alpha f} \tag{4.40}$$

in the (f, g) phase plane.

Majda *et al* [9], stimulated by a suggestion from Professor Cheng at MIT obtained the integral

$$H = \frac{1}{2}\Omega + \alpha \ln|\Omega| - \frac{\alpha^2}{2\Omega} - \frac{r^2}{2\Omega} \tag{4.41}$$

of equation (4.40), where

$$\Omega = f - g - \alpha \qquad r^2 = f^2 + g^2. \tag{4.42}$$

Introducing the variables

$$q = af + (1-a)g \qquad p = \frac{1}{f - g - \alpha} \tag{4.43}$$

where a is an arbitrary constant, equations (4.39) may be cast in the Hamiltonian form:

$$\begin{aligned} \frac{\mathrm{d}p}{\mathrm{d}t} &= -\frac{\partial H}{\partial q} \equiv -\frac{f+g}{f-g-\alpha} \\ \frac{\mathrm{d}q}{\mathrm{d}t} &= \frac{\partial H}{\partial p} \equiv -[a(f^2 - \alpha g) + (1-a)(g^2 + \alpha f)] \end{aligned} \tag{4.44}$$

where the Hamiltonian H is given by equation (4.41). The above concludes our discussion of the Hamiltonian and Lagrangian variational formulations of the solutions obtained by Majda *et al* [9]. In the next section we give numerical examples of the similarity solutions and discuss the phase plane structure of equations (4.26), (4.32) and (4.40).

5. Solution examples

In this section we investigate the phase plane structure of the similarity solutions obtained in section 4.3. The physically relevant solutions are required to be periodic in θ (a period of 2π was assumed in section 3, although this normalization for the period is not essential), and to have zero means for u and v averaged over the period. In section 5.1 we discuss solutions that depend on θ and t. We begin by discussing two solutions investigated by Majda *et al* [9] (case (*a*) $a_3 = 0$, and case (*b*) $a_1 = 0$ of section 4.3), and then go on to discuss the general similarity solutions with $a_1 \neq 0$ and $a_3 \neq 0$. Section 5.2 discusses how the solutions of section 5.1 may be generalized to include a dependence on the slow space variable x.

5.1. Solutions dependent on θ and t

5.1.1. Case $a_3 = 0$. The solutions of interest are the travelling wave solutions with similarity variable $\eta = \theta - \lambda t$, described by equations (4.29)–(4.33). Figure 1 shows the contours of the Hamiltonian

$$H_0 = \tfrac{1}{3}(u^3 + v^3) - \tfrac{1}{2}\lambda(u^2 + v^2) \tag{5.1}$$

in the (u, v)-plane (see also [9], figure 30). There are four critical points of the differential equations (4.31) and (4.32), namely the points $A(0,0)$, $B(\lambda,0)$, $C(\lambda,\lambda)$ and $D(0,\lambda)$ in figure 1. The detailed structure of the trajectories in the vicinity of the critical points may be ascertained by linearizing equation (4.32) about these points. The points A and C are centres, whereas points B and D are saddles. The orbits of most physical interest in figure 1 are the periodic orbits enclosed within the critical contour EFBDE ($H_0 = -\lambda^3/6$). From equations (4.31):

$$v = \frac{1}{\alpha}\frac{\mathrm{d}}{\mathrm{d}\eta}\left(\frac{(u-\lambda)^2}{2}\right) \qquad u = -\frac{1}{\alpha}\frac{\mathrm{d}}{\mathrm{d}\eta}\left(\frac{(v-\lambda)^2}{2}\right). \tag{5.2}$$

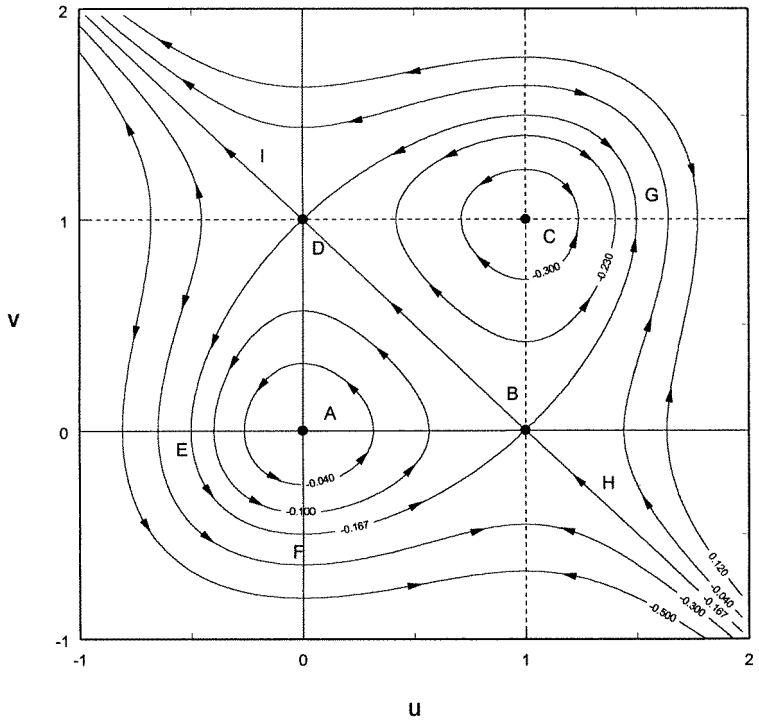

Figure 1. Contours of the Hamiltonian (5.1) for the travelling wave solutions of equations (4.29)–(4.32) corresponding to a saw-tooth entropy wave profile for the case $\lambda = 1$. The critical contours DEFBD and GBDG have a height of $H = H_c = -\lambda^3/6$.

Hence, the periodic orbits within EFBDE have zero means $\langle u \rangle$ and $\langle v \rangle$. Note that the orbits about the other centre critical point C do not have zero means, since $\mathrm{d}u/\mathrm{d}\eta$ and $\mathrm{d}v/\mathrm{d}\eta$ diverge as $u \to \lambda$ and $v \to \lambda$ respectively. This accounts for the reversal of the orbits about the horizontal line $v = \lambda$ and vertical line $u = \lambda$.

The equation of the critical contour $H_c = -\lambda^3/6$ that passes through the critical points $B(\lambda, 0)$ and $D(0, \lambda)$ consists of the straight line

$$u + v = \lambda \tag{5.3}$$

connecting the critical points, and the curved part of the contour described by the algebraic curve

$$u^2 + v^2 - uv - \tfrac{1}{2}\lambda(u + v + \lambda) = 0. \tag{5.4}$$

It is of interest to note that the periodic orbits that lie within the critical contour EFBDE have contour heights in the range $-\lambda^3/6 < H_0 < 0$, where the contour height $H_0 = 0$ corresponds to the centre critical point A.

One can show that the period T of the periodic orbits within EFBDE is a monotonic increasing function of H_0, of the form $T = (\lambda/\alpha)\tau(H_0/H_c)$ where $H_c = -\lambda^3/6$ is the value of H_0 for the critical contour. The smallest period orbit is for the orbit EFBDE, and the largest period is obtained for the limiting, zero radius orbit about A. The periodic orbits, and an expression for T are discussed in more detail in the appendix.

Figure 2 shows plots of $u(\eta)$ and $v(\eta)$ for a periodic travelling wave solution with $H_0 = -0.13$, $\alpha = 1$, $\lambda = 1.05$, for which the wave period $T = 2\pi$. Note the periodic

exchange of energy between the two sound waves. The travelling wave corresponding to the orbit EFBDE in figure 1, has a cusp in the profile of $u(\eta)$ corresponding to point D in figure 1. It is of interest to note that the conservation of H_0 throughout the motion is related to the θ-translation conservation law:

$$\frac{\partial}{\partial t}\left[\frac{1}{2}(u^2+v^2)\right]+\frac{\partial}{\partial \theta}\left[\frac{1}{3}(u^3+v^3)\right]=0 \tag{5.5}$$

obtained in equation (4.14). Equation (5.5) is the wave action conservation law, and is also related to the Manley–Rowe relations (2.16). Thus, the constancy of H_0 throughout the wave may be thought of as a balance between the conserved action density $E_2=\frac{1}{2}(u^2+v^2)$ and the action flux $F_2=\frac{1}{3}(u^3+v^3)$.

5.1.2. Case $a_1=0$. The solutions of interest in this case are described by equations (4.38)–(4.42), namely

$$u=f(t)(\theta-\theta_0) \qquad v=g(t)(\theta-\theta_0) \qquad |\theta-\theta_0|<\pi \tag{5.6}$$

extended periodically in θ with a period of 2π. These solutions have an array of shocks located at $\theta=\theta_0+(2n+1)\pi$ where n takes on integer values. The solutions for f and g satisfy equations (4.39):

$$f'(t)=-(f^2-\alpha g) \qquad g'(t)=-(g^2+\alpha f) \qquad \frac{\mathrm{d}g}{\mathrm{d}f}=\frac{g^2+\alpha f}{f^2-\alpha g}. \tag{5.7}$$

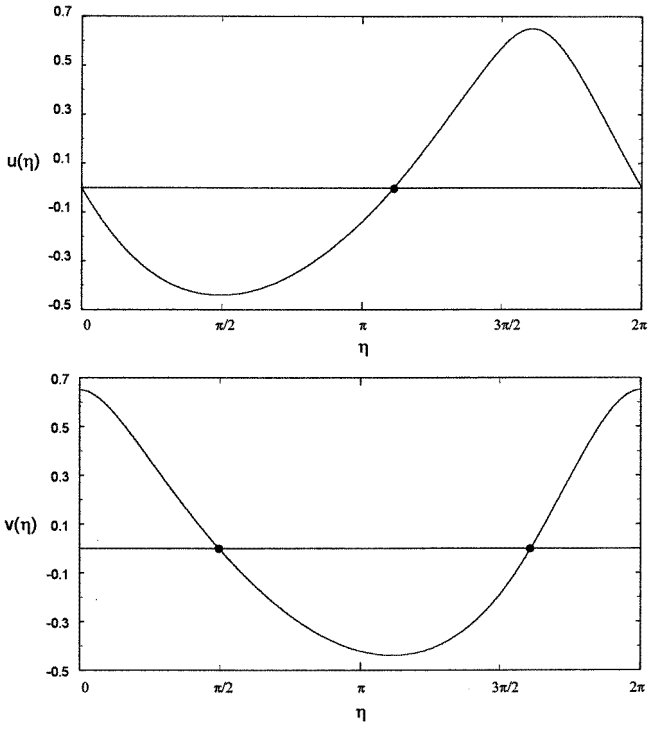

Figure 2. Plots of u and v versus η for a periodic travelling wave solution described by equations (5.1) and (5.2). The Hamiltonian has a value of $H_0=-0.13$, $\alpha=1$ and $\lambda=1.05$. The period of the wave in θ or η is $T=2\pi$.

This solution was studied by Majda *et al* [9].

At a shock in u and v, the Rankine Hugoniot conditions for equations (4.1) and (4.2) require that the shock speed satisfy

$$s = \tfrac{1}{2}(u_- + u_+) \qquad \text{and/or} \qquad s = \tfrac{1}{2}(v_- + v_+) \tag{5.8}$$

where $u_\pm = u(\theta_{s\pm}, t)$, $v_\pm = v(\theta_{s\pm}, t)$ denote the values of u and v on either side of the shock located at $\theta = \theta_s$. The Lax entropy conditions (Lax [18]; Chorin and Marsden [19]) require either $u_- > u_+$ or $v_- > v_+$ or both $u_- > u_+$ and $v_- > v_+$ at the shock. In the present case of adiabatic gas dynamics, the Lax entropy conditions are equivalent to the requirement that the shock is compressive. The conditions $u_- > u_+$ and/or $v_- > v_+$ used in conjunction with the wave action integral (2.16) with $m = 1$ and $n = -1$ requires

$$\frac{\partial}{\partial t}\left(\int_0^{2\pi} \frac{u^2 + v^2}{2}\,\mathrm{d}\theta\right) = -\sum_s \left[\frac{u^3 + v^3}{3}\right]_{\theta_{s+}}^{\theta_{s-}} < 0 \tag{5.9}$$

so that the wave action integral is a decreasing function of time, owing to the presence of shocks. The entropy conditions in the present example require

$$f(t) \geqslant 0 \qquad \text{and} \qquad g(t) \geqslant 0. \tag{5.10}$$

Conditions (5.10) appear to be unnecessarily restrictive, since the wave action will decay if the right-hand side of equation (5.9) is negative definite.

Figure 3 shows contours of the Hamiltonian integral (4.41) of equations (5.7) in the (f, g) phase plane for the case $\alpha = 1$ (compare with figure 1 of [9]). The autonomous differential equation system (5.7) in the (f, g) phase plane has a centre critical point at

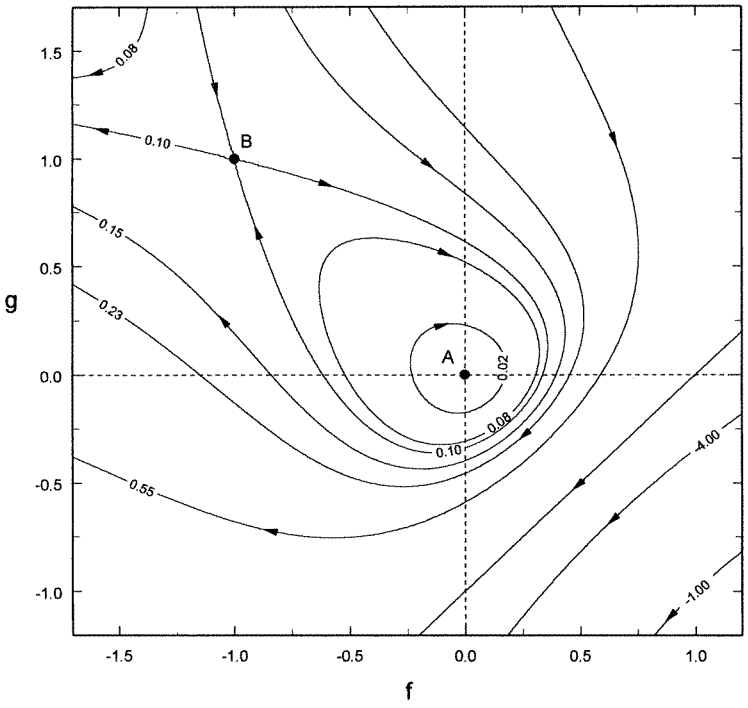

Figure 3. Contours of the Hamiltonian integral (4.41) for the periodic N-wave solution obtained by Majda *et al* [9] described by equations (5.6) and (5.7) for the case $\alpha = 1$.

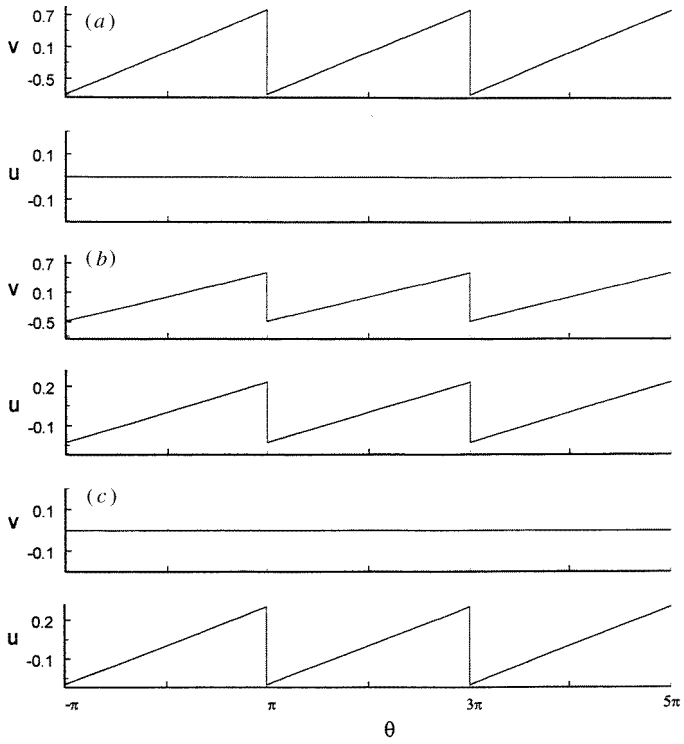

Figure 4. A schematic diagram of the evolution of an N-wave, periodic shock solution described by equations (5.6) and (5.7), where the parameter $\theta_0 = 0$. The shocks occur at $\theta_s = (2s+1)\pi$ (s integer), and correspond to the Hamiltonian contour height $H_0 = 0.015$ displayed in figure 3.

$A(0,0)$ and a saddle critical point at $B(-\alpha,\alpha)$. Note that $g = f - \alpha$ is a special solution of the equation for $\mathrm{d}g/\mathrm{d}f$ in equations (5.7). The Hamiltonian integral (4.41) diverges as $g \to (f-\alpha)$, with $H \to +\infty$ as $g \to (f-\alpha)_+$ but $H \to -\infty$ as $g \to (f-\alpha)_-$. Figure 4 shows the evolution of an N-wave periodic shock solution for $\theta_0 = 0$. Shocks occur at $\theta_s = (2s+1)\pi$ (s integer) and the amplitude of the wave is determined by the $H = 0.15$ contour in figure 5 at three different values of t, with $t = 0$ corresponding to the instant when $f = 0$ and $g > 0$ (case (a)), $t = t_{\rm crit}$ when $g = 0$ and $f > 0$ (case (c)), and at an intermediate time t_I: $0 < t_I < t_{\rm crit}$ (case (b)). At time $t = 0$, $u \equiv 0$, and v consists of an N-wave profile in θ with shocks. As time increases the forward wave u develops into an N-wave as part of the energy in the backward wave is transferred to the forward wave u. At some later time $t = t_{\rm crit}$, u is a fully developed N-wave and $u \equiv 0$. The shocks in this model have zero speed $s = 0$. Majda *et al* [9] argue that after the critical time when $g = 0$ (when the entropy conditions (5.10) first fail), the solution evolves into a cusped rarefaction wave. They also argue that since the shocks in u and v are locked together, the solution is structurally unstable to perturbations.

5.1.3. Case $a_1 \neq 0$ and $a_3 \neq 0$. In this case the similarity solutions for u and v are given by equations (4.23)–(4.26), namely

$$u = (\theta - \theta_0) f(\eta) \qquad v = (\theta - \theta_0) g(\eta) \tag{5.11}$$

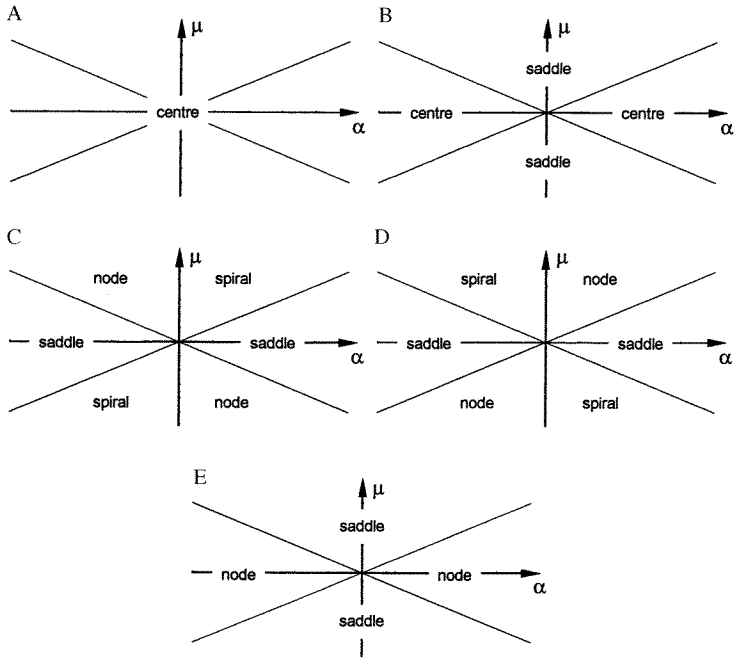

Figure 5. Schematic diagram of the character of the critical points of the differential equation (5.13) for $\mathrm{d}g/\mathrm{d}f$ depending on the parameters (α, μ). The critical points in the (f, g) phase plane are located at the points $A(0, 0)$, $B(\mu, \mu)$, $C(\mu, \mu^2/\alpha)$, $D(-\mu^2/\alpha, \mu)$ and $E(-\alpha, \alpha)$. The points are either saddles, centres, spirals or nodes. The parameter space is split up into eight sectors by the lines $\mu = 0$, $\alpha = 0$ and $\mu = \pm\alpha$.

where

$$\eta = \ln|\theta - \theta_0| - \mu t \qquad \mu = \frac{a_3}{a_1} \qquad \theta_0 = -\frac{a_2}{a_3} \tag{5.12}$$

and f and g satisfy the differential equations:

$$f'(\eta) = -\frac{f^2 - \alpha g}{f - \mu} \qquad g'(\eta) = -\frac{g^2 + \alpha f}{g - \mu} \qquad \frac{\mathrm{d}g}{\mathrm{d}f} = \frac{(g^2 + \alpha f)(f - \mu)}{(f^2 - \alpha g)(g - \mu)} \equiv \frac{N}{D} \tag{5.13}$$

where the last equation describes the solution trajectories in the (f, g) phase plane.

Before discussing the phase plane trajectories of equations (5.13) it is instructive to consider the limiting behaviour of the similarity variable η in the limits where $a_1 \to 0$ and $a_3 \to 0$.

5.1.4. Limit $a_3 \to 0$. Consider the rescaled similarity variable η_T^*:

$$\eta_T^* = \frac{\lambda}{\mu}\left(\eta - \ln\left|\frac{\lambda}{\mu}\right|\right) \qquad \lambda = -\theta_0\mu \qquad \lim_{\mu\to 0}\eta_T^* = \theta - \lambda t. \tag{5.14}$$

Note that in the limit as $\mu \to 0$, the variable η_T^* becomes the the similarity variable for the travelling wave solution of equations (4.29)–(4.32).

The solutions (4.23)–(4.26) for u and v may be written in the form:

$$\begin{aligned} u &= F(\eta_T^*)\exp(\mu t) \qquad & F(\eta_T^*) &= -\sigma\exp(\eta) f(\eta) \\ v &= G(\eta_T^*)\exp(\mu t) \qquad & G(\eta_T^*) &= -\sigma\exp(\eta) g(\eta) \end{aligned} \tag{5.15}$$

where $\sigma = \mathrm{sgn}(\theta_0)$ is the sign of θ_0 and F and G satisfy the equations:

$$\frac{\mathrm{d}F}{\mathrm{d}\eta^*} = \frac{\alpha G - \mu F}{\exp(-\mu\eta^*/\lambda)F - \lambda} \qquad \frac{\mathrm{d}G}{\mathrm{d}\eta^*} = -\frac{\alpha F + \mu G}{\exp(-\mu\eta^*/\lambda)G - \lambda} \tag{5.16}$$

where we use the notation $\eta^* \equiv \eta_T^*$. Letting $\mu \to 0$, equations (5.16) reduce to the travelling wave equations (4.31) for $u \equiv F(\eta^*)$ and $v \equiv G(\eta^*)$.

5.1.5. Limit $a_1 \to 0$. In this limit we consider the rescaled similarity variable η_N^*, and functions $\hat{F}(\eta_N^*)$ and $\hat{G}(\eta_N^*)$:

$$\eta_N^* = -\frac{\eta}{\mu} \qquad \lim_{\mu\to\infty} \eta_N^* = t \qquad \hat{F}(\eta_N^*) = f(\eta) \qquad \hat{G}(\eta_N^*) = g(\eta). \tag{5.17}$$

In the limit as $\mu \to \infty$ the functions $\hat{F}$ and $\hat{G}$ satisfy the differential equations (4.39) for the N-wave solutions of [9].

5.1.6. Phase plane trajectories. The differential equation (5.13) for $\mathrm{d}g/\mathrm{d}f$ in general has five critical points in the (f, g) phase plane where the numerator N and denominator D on the right-hand side of equation (5.13) for $\mathrm{d}g/\mathrm{d}f$ are simultaneously zero. The character of the critical points depends on the relative values of α and μ. The critical points are located at the points $A(0, 0)$, $B(\mu, \mu)$, $C(\mu, \mu^2/\alpha)$, $D(-\mu^2/\alpha, \mu)$ and $E(-\alpha, \alpha)$. The character of the critical points may be determined by linearizing the differential equations (5.13) about the critical points. A schematic diagram of the character of the critical points depending on the values of α and μ is given in figure 5. Linearizing the differential equation (5.13) about the critical points shows that: $A(0, 0)$ is a centre; $B(\mu, \mu)$ is a centre if $\mu^2 < \alpha^2$ but

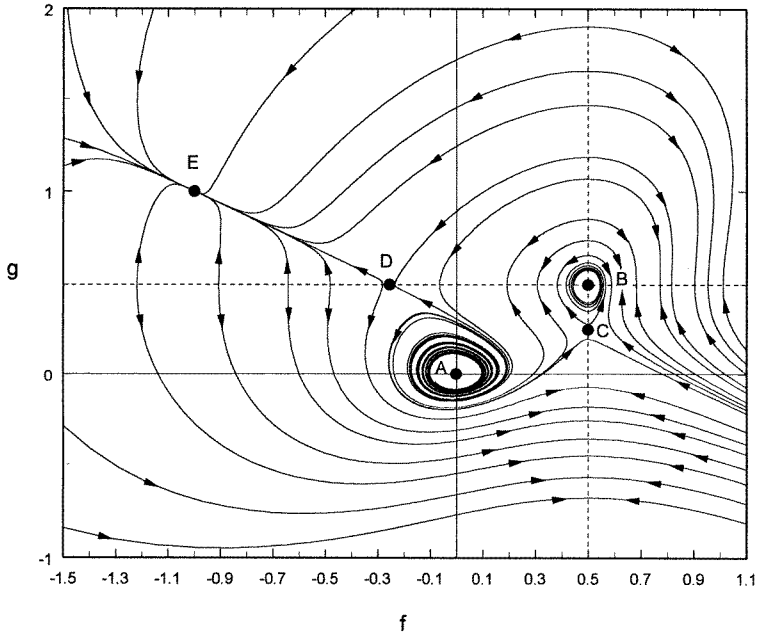

Figure 6. Phase plane trajectories of the differential equation system (5.13) in the (f, g) plane for the case $\mu = 0.5$ and $\alpha = 1$. The corresponding similarity solutions for u and v are given by equations (5.11).

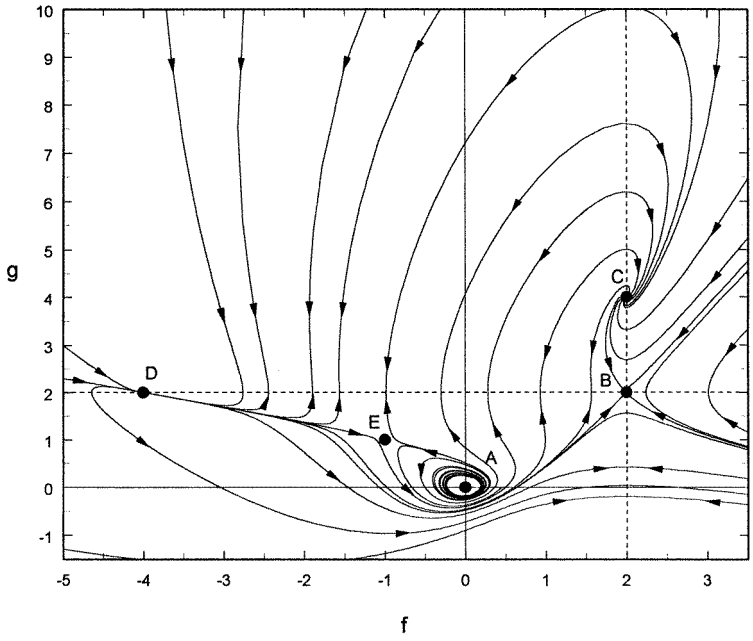

Figure 7. Same as in figure 6 except $\mu = 2$ and $\alpha = 1$.

a saddle if $\mu^2 > \alpha^2$; point $E(-\alpha, \alpha)$ is a node if $\mu^2 < \alpha^2$, but a saddle if $\mu^2 > \alpha^2$. Points C and D are more complicated in their behaviour. Point $C(\mu, \mu^2/\alpha)$ is a spiral point in the parameter regime between the μ-axis and the line $\mu = \alpha$ (i.e. $0 < \alpha < \mu$ or $\mu < \alpha < 0$); a node if (α, μ) lies in the regime between the μ-axis and the line $\mu = -\alpha$ (i.e. $-\mu < \alpha < 0$ or $0 < \alpha < -\mu$), and a saddle if $|\alpha| > |\mu|$. Similarly, point $D(-\mu^2/\alpha, \mu)$ is a node if (α, μ) lies in the region between the μ-axis and the line $\mu = \alpha$; a spiral point if (α, μ) lies in the region between the μ-axis and the line $\mu = -\alpha$; and a saddle if $|\alpha| > |\mu|$.

Figures 6 and 7 show typical phase space plots for f and g obtained by solving the differential equations (5.13). Figure 6 shows phase plane trajectories for the case $\alpha = 1$ and $\mu = 0.5$. The critical point A is a centre; B is a centre; points C and D are saddles, and point E is a node. The phase plane trajectories are similar in many respects to the travelling wavephase plane trajectories in figure 1.

Figure 7 shows the phase plane trajectories for the differential equation system (5.13) for a case in which $\mu > \alpha$, namely $\mu = 2$ and $\alpha = 1$. In this case linear critical point analysis indicates that $A(0, 0)$ is a centre, $B(\mu, \mu)$ is a saddle, $C(\mu, \mu^2/\alpha)$ is a spiral, $D(-\mu^2/\alpha, \mu)$ is a node and $E(-\alpha, \alpha)$ is a saddle. Note that the trajectories about $A(0, 0)$ are spirals. The phase plane trajectories about A are somewhat similar to those for the N-wave periodic shock solution displayed in figure 3 ($\mu \to \infty$, $\theta_0 = -\lambda/\mu$ fixed, $\alpha = 1$).

Figure 8 shows plots of the similarity solutions for $u(\theta, t)$ and $v(\theta, t)$ versus θ at two time instants $t = 0$ and $t = t_1 = 10\ln(1.25) = 2.231$ using the parameters $\lambda = -0.1\pi$, $\mu = 0.1$ and $\alpha = 1$. The full curves give $u(\theta, 0)$ and $v(\theta, 0)$ whereas $u(\theta, t_1)$ and $v(\theta, t_1)$ are given by the broken curves. For $\mu > 0$, the wave progresses outwards from the central point $\theta = \pi$ in both directions and grows in amplitude as it progresses. Linearizing

equations (5.16) yield the approximate small amplitude solutions

$$u(\theta,t) = r_0\left|\frac{\theta-\theta_0}{\theta_0}\right|\sin\left(\frac{\alpha}{\mu}\ln\left|\frac{\theta-\theta_0}{\theta_0}\right| - \alpha t\right)$$
$$v(\theta,t) = r_0\left|\frac{\theta-\theta_0}{\theta_0}\right|\cos\left(\frac{\alpha}{\mu}\ln\left|\frac{\theta-\theta_0}{\theta_0}\right| - \alpha t\right) \tag{5.18}$$

for u and v, which are similar to the solutions for u and v displayed in figure 8. The solutions in figure 8 do not have zero means with respect to θ averaged from $\theta = 0$ to $\theta = 2\pi$. However, it may be possible to construct physically relevant solutions of the above form that are periodic with period 2π in θ and with zero means with respect to θ, by inserting shocks. In any event the type of solutions described by figures 6–8 show how the travelling wave solutions (figures 1 and 2), and the N-wave, periodic shock solutions (figures 3 and 4) are special limits of the more general solutions of figures 6–8.

5.2. Solutions dependent on θ, t and x

The solutions dependent on θ and t, discussed in section 5.1, can be generalized to include a dependence on the long space variable x. For the case of a periodic saw-tooth entropy wave profile (equation (2.19)), the solutions for the backward and forward wave velocity perturbations u and v satisfy equations (2.21) and (2.22). Equations (2.21) and (2.22) admit solutions of the form:

$$u = u(z,\theta) \qquad v = v(z,\theta) \tag{5.19}$$

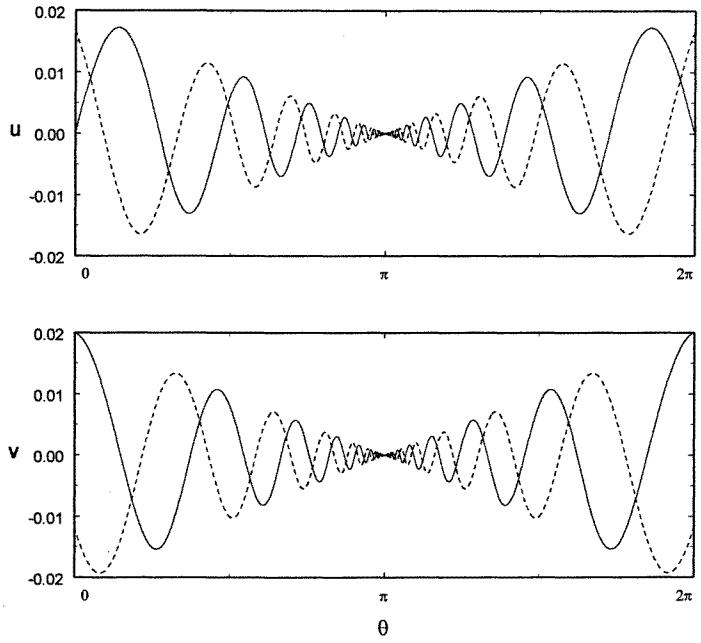

Figure 8. Plots of $u(\theta,t)$ and $v(\theta,t)$ versus θ corresponding to the similarity solutions (5.15), for two time instants $t = 0$ (full curve) and $t = t_1 = 2.231$ (broken curve) in which $F(\eta^*)$ and $G(\eta^*)$ satisfy equations (5.16). The solutions for $F(\eta^*)$ and $G(\eta^*)$ are for $\mu = 0.1$, $\lambda = -0.1\pi$, $\alpha = 1$, with $F = 0$ and $G = 0.02$ at $\eta^* = 0$.

where

$$z = \nu x + \omega t \tag{5.20}$$

and ν and ω are constants. The solutions of section 5.1 correspond to solutions of the form of (5.19) in which $\nu = 0$ and $\omega = 1$. Solutions of the so-called signalling problem in which $u = u(x, \theta)$ and $v = v(x, \theta)$ have been discussed by Anile *et al* [7].

Substituting the solution ansatz (5.19) and (5.20) into equations (2.21) and (2.22) results in the equations

$$\begin{aligned}&(\omega + \nu)u_z + uu_\theta - \alpha v = 0\\ &(\omega - \nu)v_z + vv_\theta + \alpha u = 0.\end{aligned} \tag{5.21}$$

Equations (5.21) admit the same infinitesimal Lie point symmetries as the Lie point symmetries of the θ and t dependent solutions discussed in equations (4.6)–(4.9), except t is replaced by z. Hence, equations (5.21) admit similarity solutions analogous to the (θ, t) dependent solutions discussed in sections 4 and 5.1.

The simplest solutions of equations (5.21) are probably the travelling wave solutions of the form

$$u = u(\eta) \qquad v = v(\eta) \tag{5.22}$$

where

$$\eta = \theta - \lambda z \equiv \theta - \lambda(\nu x + \omega t) \tag{5.23}$$

is the similarity variable and λ is a constant. Substituting the solution ansatz (5.22) and (5.23) into equations (5.21) yields the ordinary differential equations:

$$[u - \lambda(\omega + \nu)]u'(\eta) = \alpha v \qquad [v - \lambda(\omega - \nu)]v'(\eta) = -\alpha u \tag{5.24}$$

for u and v. From equations (5.24)

$$\frac{\mathrm{d}u}{\mathrm{d}v} = -\frac{v[v - \lambda(\omega - \nu)]}{u[u - \lambda(\omega + \nu)]} \tag{5.25}$$

is the form of the corresponding differential equation for the solution trajectories in the (u, v) phase plane. Equations (5.25) have the Hamiltonian integral

$$H = \tfrac{1}{3}(u^3 + v^3) - \tfrac{1}{2}\lambda[(\omega + \nu)u^2 + (\omega - \nu)v^2]. \tag{5.26}$$

One pair of canonical variables (q, p) for the Hamiltonian system of differential equations (5.24), with Hamiltonian (5.26) are:

$$q = \frac{a[u - \lambda(\omega + \nu)]^2}{2\alpha^{\frac{1}{2}}} \qquad p = \frac{[v - \lambda(\omega - \nu)]^2}{2\alpha^{\frac{1}{2}}a} \tag{5.27}$$

where a is an arbitrary constant. The canonical variables (5.27) are the natural generalization of the canonical variables (q_1, p_1) of equations (4.34) for the (θ, t)-dependent travelling wave solutions discussed in sections 4.3 and 5.1.

Figures 9 and 10 show examples of phase plane plots of the solutions of equations (5.24) and (5.25) for two representative cases. Figure 9 shows a case in which $\omega > \nu > 0$ ($\omega = 1$, $\nu = 0.7$ and $\lambda = 1$), which corresponds in the long scale sense to a supersonic travelling wave moving in the negative x-direction with phase velocity $\boldsymbol{V}_p = -1.4286c\boldsymbol{e}_x$ where c is the gas sound speed (see equation (5.23)). Figure 10 shows a further example that corresponds in the long scale sense to a subsonic travelling wave moving in the negative x-direction ($\omega = 0.7$, $\nu = 1$, and $\lambda = 1$), with phase velocity $\boldsymbol{V}_p = -0.7c\boldsymbol{e}_x$. Figures 9 and 10 and equation (5.25) have four critical points in the (u, v) phase plane located at $A(0, 0)$,

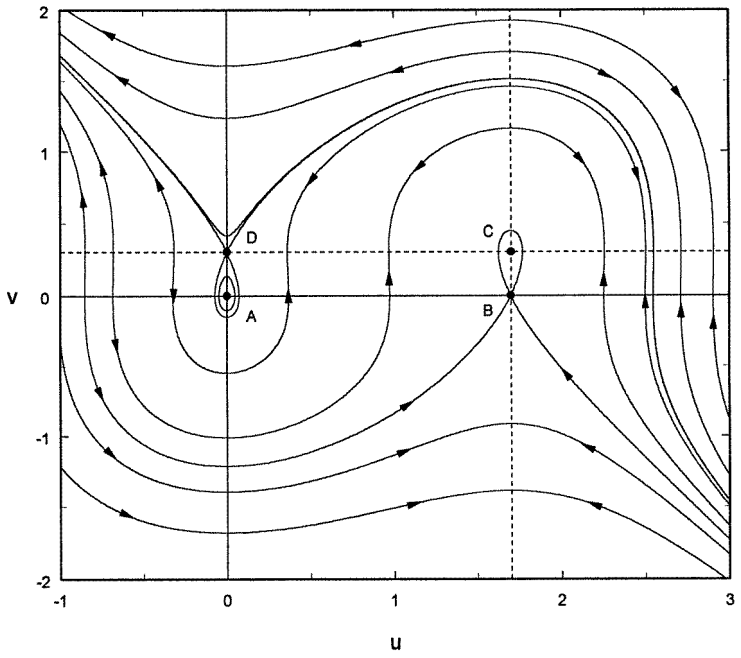

Figure 9. Contours of the Hamiltonian integral (5.26) corresponding to the travelling wave similarity solution of equations (5.22)–(5.24) for the parameter values $\omega = 1$, $\nu = 0.7$ and $\lambda = 1$. The solution depends on θ, x and t and corresponds to a supersonic travelling wave with velocity $\boldsymbol{V}_p = -1.4286c\boldsymbol{e}_x$ where c is the sound speed.

$B[\lambda(\omega+\nu), 0]$, $C[\lambda(\omega+\nu), \lambda(\omega-\nu)]$ and $D[0, \lambda(\omega-\nu)]$. In the supersonic case $\omega^2 > \nu^2$, A and C are centres, and B and D are saddles. The solution trajectories in figure 9 are quite distinct from the travelling wave phase portraits for the case $\omega = 1$, $\nu = 0$ and $\lambda = 1$ displayed in figure 1 (in figure 1 $V_p = 0$). In figure 9 the critical contours passing through the saddles B and D are of different height, and there is no trajectory joining the saddles as in figure 1. Smooth, periodic travelling waves in figure 9 with zero means for u and v averaged over one period in θ, are represented by the closed contours that encircle the centre critical point at A. In the subsonic case displayed in figure 10 for which $\omega^2 < \nu^2$, A and C are saddles and B and D are centres. In this latter case there are no smooth travelling wave solutions with zero means for u and v, since the critical point $A(0, 0)$ is a saddle and there are no trajectories that can encircle the origin $A(0, 0)$. For the sonic case $\omega = \pm\nu$, the critical points coalesce into two pairs of critical points to form critical points that are a hybrid between a centre and a saddle. Thus, as $V_p \downarrow c$ the amplitude of the smooth travelling wave solutions tends to zero.

6. Hamiltonian equations in Fourier space

In this section we consider the form of the resonant-wave interaction equations (3.1) and (3.2) for the case of solutions that are independent of the long space variable x, and for the case $m = 1$ and $n = -1$. In this case the equations for the sound waves can be expressed

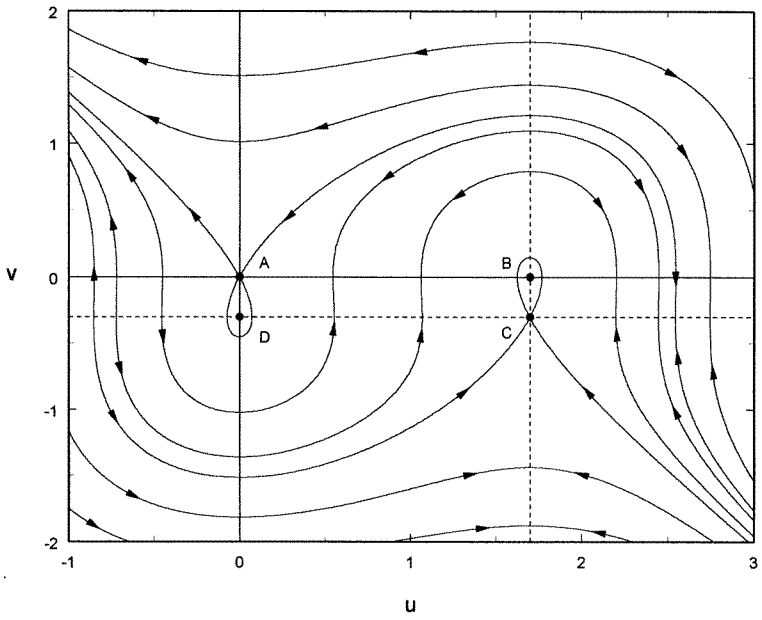

Figure 10. Same as in figure 9 except for the case of a subsonic solution with $\omega = 0.7$, $\nu = 1$ and $\lambda = 1$. The wave velocity $\boldsymbol{V}_p = -0.7c\boldsymbol{e}_x$, where c is the sound speed.

in the Hamiltonian form:

$$u_t = D_\theta \left(\frac{\delta H}{\delta u} \right) \qquad v_t = D_\theta \left(\frac{\delta H}{\delta v} \right) \tag{6.1}$$

where the Hamiltonian functional H from equation (3.13) may be split into quadratic (H_0) and cubic (H_1) terms:

$$\begin{aligned} H &= H_0 + H_1 \\ H_0 &= \int_0^{2\pi} \mathrm{d}\theta \, \tfrac{1}{2}[v\hat{K}^\dagger(D_\theta^{-1}u) - u\hat{K}(D_\theta^{-1}v)] \\ H_1 &= -\int_0^{2\pi} \mathrm{d}\theta \, \tfrac{1}{6}(u^3 + v^3) \end{aligned} \tag{6.2}$$

and the integral operators $\hat{K}$ and $\hat{K}^\dagger$ are defined in equations (3.3) and (3.4). The term H_0 in equations (6.2) represents linear dispersive wave effects associated with three-wave resonant interactions, and H_1 consists of the Burgers' self-wave interaction terms.

Since the solutions for u and v of equations (3.1) and (3.2) (or equations (6.1) and (6.2)) are assumed to be 2π-periodic in θ with zero means, it is natural to investigate the Fourier space decomposition of the solutions with respect to θ by using the Fourier expansions:

$$u(\theta, t) = \sum_{p=-\infty}^{\infty} u_p(t) \exp(\mathrm{i}p\theta) \qquad v(\theta, t) = \sum_{p=-\infty}^{\infty} v_p(t) \exp(\mathrm{i}p\theta) \tag{6.3}$$

where the Fourier coefficients $\{u_p(t)\}$ and $\{v_p(t)\}$ are given by the formulae:

$$u_p(t) = \frac{1}{2\pi} \int_0^{2\pi} u(\theta, t) \exp(-\mathrm{i}p\theta) \, \mathrm{d}\theta \qquad v_p(t) = \frac{1}{2\pi} \int_0^{2\pi} v(\theta, t) \exp(-\mathrm{i}p\theta) \, \mathrm{d}\theta \tag{6.4}$$

and the variable p takes on only integer values. Note that $u_0 = 0$ and $v_0 = 0$ in equations (6.3) since u and v have zero means. In Fourier space, equations (3.1) and (3.2) reduce to

$$\begin{aligned}\frac{\partial u_s}{\partial t} &= -\frac{\mathrm{i}s}{2}\sum_{p=-\infty}^{\infty} u_p u_{s-p} - K_s v_s \\ \frac{\partial v_s}{\partial t} &= -\frac{\mathrm{i}s}{2}\sum_{p=-\infty}^{\infty} v_p v_{s-p} + K_{-s} u_s\end{aligned} \tag{6.5}$$

where

$$K_s = \frac{1}{2\pi}\int_0^{2\pi} K(\theta)\exp(-\mathrm{i}s\theta)\,\mathrm{d}\theta \tag{6.6}$$

denotes the sth Fourier coefficient of $K(\theta)$. Note that for the periodic saw-tooth entropy profile case K_s is given by

$$K_s = K_{-s} = -\alpha. \tag{6.7}$$

Although the Dirac delta distribution (2.20) for $K(\theta)$ is not a square integrable equation, (6.6) still yields the correct formula (6.7) for K_s. Since $u(\theta, t)$, $v(\theta, t)$ and $K(\theta)$ are real it is necessary that the Fourier coefficients satisfy the equations:

$$u_s^* = u_{-s} \qquad v_s^* = v_{-s} \qquad K_s^* = K_{-s} \tag{6.8}$$

where the superscript $*$ denotes the complex conjugate.

The main aim of the present development is first to determine the form of Hamilton's equations in Fourier space (section 6.1). The equations are then transformed to normal form (see for example [20, 21]), in order to isolate the normal modes of the system (section 6.2). Further canonical transformations can then be carried out to further investigate the equations.

6.1. Hamilton's equations in Fourier space

Using the Fourier representations (6.3) for u and v (and a similar representation for $K(\theta)$), the Hamiltonian functionals H_0 and H_1 may be expressed as

$$H_0 = \mathrm{i}\pi \sum_{p=-\infty}^{\infty}{}' \frac{K_p v_p u_{-p} - K_{-p} v_{-p} u_p}{p} \tag{6.9}$$

$$H_1 = -\frac{\pi}{3}\sum_{s=-\infty}^{\infty}{}' \sum_{p=-\infty}^{\infty}{}' (u_s u_p u_{-s-p} + v_s v_p v_{-s-p}) \tag{6.10}$$

where the Fourier coefficients $\{u_s, v_s, K_s\}$ satisfy the reality constraints (6.8). The superscript $'$ on the sums in equations (6.9) and (6.10) denote sum over all integers excluding $p = 0$ and $s = 0$.

Noting that $H = H_0 + H_1$, straightforward computation of $\delta H/\delta u_s^*$ and $\delta H/\delta v_s^*$ yields Hamilton's equations in Fourier space as

$$\frac{\partial u_s}{\partial t} = \frac{\mathrm{i}s}{2\pi}\frac{\delta H}{\delta u_s^*} = -\frac{\mathrm{i}s}{2}\sum_{p=-\infty}^{\infty} u_p u_{s-p} - K_s v_s \tag{6.11}$$

$$\frac{\partial v_s}{\partial t} = \frac{\mathrm{i}s}{2\pi}\frac{\delta H}{\delta v_s^*} = -\frac{\mathrm{i}s}{2}\sum_{p=-\infty}^{\infty} v_p v_{s-p} + K_{-s} u_s. \tag{6.12}$$

Equations (6.11) and (6.12) imply that $\{u_s, u_s^*\}$ and $\{v_s, v_s^*\}$ are canonically conjugate variables.

6.2. Reduction to normal form

Consider the linearized form of Hamilton's equations (6.11) and (6.12):

$$\begin{aligned}\frac{\partial u_s}{\partial t} &= \frac{\mathrm{i}s}{2\pi}\frac{\delta H_0}{\delta u_s^*} = -K_s v_s \\ \frac{\partial v_s}{\partial t} &= \frac{\mathrm{i}s}{2\pi}\frac{\delta H_0}{\delta v_s^*} = K_s^* u_s.\end{aligned} \tag{6.13}$$

Note that the linearized equations (6.13) have solutions for u_s and v_s that satisfy the equations:

$$\frac{\partial^2 u_s}{\partial t^2} + |K_s|^2 u_s = 0 \qquad \frac{\partial^2 v_s}{\partial t^2} + |K_s|^2 v_s = 0. \tag{6.14}$$

For normal coordinates $\{a_s\}$ we require $\partial a_s/\partial t = \mathrm{i}|K_s|a_s$ and that $\{a_s\}$ are canonical coordinates. Thus, normal coordinates allow the identification of the different linear wave modes in the system.

Following the approach of Zakharov and Kuznetsov [20] and Zakharov *et al* [21], we consider transformations of the form:

$$\begin{pmatrix} u_s \\ v_s \end{pmatrix} = \begin{pmatrix} \alpha_s & \alpha_{-s}^* \\ \beta_s & \beta_{-s}^* \end{pmatrix} \begin{pmatrix} a_s \\ a_{-s}^* \end{pmatrix} \tag{6.15}$$

where $\{a_s\}$ and $\{a_s^*\}$ are normal variables. Note that transformations (6.15) automatically ensure that $u_s^* = u_{-s}$ and $v_s^* = v_{-s}$ as required by the reality constraints (6.8) for u and v. It turns out that one can choose the coefficients $\{\alpha_s\}$ and $\{\beta_s\}$ in equations (6.15) so that the $\{a_s\}$ satisfy Hamilton's equations:

$$\frac{\partial a_s}{\partial t} = \mathrm{i}\,\mathrm{sgn}(s)\frac{\delta H_0}{\delta a_s^*} = \mathrm{i}|K_s|a_s \tag{6.16}$$

for the normal variables, where $\mathrm{sgn}(s)$ denotes the sign of s.

The inverse of transformations (6.15) are given by:

$$\begin{aligned} a_s &= (\beta_{-s}^* u_s - \alpha_{-s}^* v_s)/J_s \\ a_{-s}^* &= (-\beta_s u_s + \alpha_s v_s)/J_s \end{aligned} \tag{6.17}$$

where

$$J_s = \alpha_s \beta_{-s}^* - \beta_s \alpha_{-s}^* \tag{6.18}$$

is the determinant of transformation (6.15). From equations (6.9) and (6.15) the Hamiltonian H_0 may be expressed as

$$H_0 = 2\pi\mathrm{i}\sum_{p=-\infty}^{\infty}{}' [K_p\beta_p\alpha_p^* - K_p^*\beta_p^*\alpha_p)a_p a_p^* + K_p\beta_p\alpha_{-p}a_p a_{-p} - K_p^*\beta_p^*\alpha_{-p}^* a_p^* a_{-p}^*]/p. \tag{6.19}$$

Computing $\partial a_s/\partial t$ using equations (6.17), (6.11) and (6.12) and computing $\delta H_0/\delta a_s^*$ using equation (6.19), we find that equations (6.16) are satisfied provided α_s and β_s are chosen so that

$$\alpha_s = \mathrm{i}\beta_{-s} \qquad J_s = \mathrm{i}[|\beta_s|^2 + |\beta_{-s}|^2] = \frac{\mathrm{i}|s|}{2\pi} \qquad \beta_{-s} = \frac{K_s}{|K_s|}\beta_s. \tag{6.20}$$

Equations (6.20) have solutions

$$\begin{aligned} \alpha_s &= \mathrm{i}\left(\frac{|s|}{4\pi}\right)^{\frac{1}{2}}\left(\frac{K_s}{|K_s|}H(s) + 1 - H(s)\right) \\ \beta_s &= \left(\frac{|s|}{4\pi}\right)^{\frac{1}{2}}\left(H(s) + \frac{K_s^*}{|K_s|}[1 - H(s)]\right) \end{aligned} \tag{6.21}$$

where $H(s)$ is the Heaviside step function.

From equations (6.15) and (6.21) the original coordinates $\{u_s\}$ and $\{v_s\}$ can be expressed in terms of the normal coordinates, by the equations:

$$u_s = \mathrm{i}\left(\frac{|s|}{4\pi}\right)^{\frac{1}{2}}\left[\left(\frac{K_s}{|K_s|}a_s - a^*_{-s}\right)H(s) + \left(a_s - \frac{K_s}{|K_s|}a^*_{-s}\right)[1-H(s)]\right]$$
$$v_s = \left(\frac{|s|}{4\pi}\right)^{\frac{1}{2}}\left[\left(a_s + \frac{K^*_s}{|K_s|}a^*_{-s}\right)H(s) + \left(\frac{K^*_s}{|K_s|}a_s + a^*_{-s}\right)[1-H(s)]\right]. \tag{6.22}$$

The inverse transformations are readily determined from (6.16).

In terms of the normal coordinates $\{a_s\}$, the Hamiltonian H_0 has the form:

$$H_0 = \sum_{s=-\infty}^{\infty}{}' \operatorname{sgn}(s)|K_s|a_s a^*_s \tag{6.23}$$

where $\omega_s = |K_s|$ are the characteristic frequencies for the $\{a_s\}$. Similarly, the cubic Hamiltonian functional H_1 in equation (6.10) may be written in terms of the normal coordinates as

$$H_1 = -\frac{\pi}{3}\sum_{k=-\infty}^{\infty}{}'\sum_{p=-\infty}^{\infty}{}'\sum_{s=-\infty}^{\infty}{}'[(U_{spk}a_s a_p a_k + U^*_{spk}a^*_s a^*_p a^*_k)\delta_{k+s+p,0}$$
$$+3(V_{spk}a_s a_p a^*_k + V^*_{spk}a^*_s a^*_p a_k)\delta_{k-s-p,0}] \tag{6.24}$$

where

$$U_{spk} = \alpha_s\alpha_p\alpha_k + \beta_s\beta_p\beta_k$$
$$V_{spk} = \alpha_s\alpha_p\alpha^*_k + \beta_s\beta_p\beta^*_k \tag{6.25}$$

and $\delta_{a,b}$ is the Kronecker delta symbol.

In terms of normal coordinates Hamilton's equations (6.11) and (6.12) may be expressed in the form:

$$\frac{\partial a_s}{\partial t} = \mathrm{i}\operatorname{sgn}(s)\frac{\delta H}{\delta a^*_s} = \mathrm{i}\Bigg[|K_s|a_s - \pi\operatorname{sgn}(s)\sum_{p=-\infty}^{\infty}{}'\sum_{k=-\infty}^{\infty}{}'(U^*_{spk}a^*_p a^*_k\delta_{k+s+p,0}$$
$$+V_{kps}a_p a_k\delta_{k+p-s,0} + 2V^*_{spk}a^*_p a_k\delta_{k-s-p,0})\Bigg]. \tag{6.26}$$

Thus $\{a_s, a^*_s\}$ are canonically conjugate pairs.

7. Summary and concluding remarks

The main theme of this paper has been the Hamiltonian structure of the equations for three-wave resonant interaction in adiabatic gas dynamics in one Cartesian space dimension derived by Majda and Rosales [1]. The equations consist of two inviscid Burgers equations for the backward and forward sound waves coupled via linear integral operators that describe the resonant reflection of a sound wave off an entropy wave disturbance to produce the reverse sound wave. The detailed form of the equations (equations (2.11) and (2.12)) depend on the resonance conditions (2.7) that relate the frequencies and wavenumbers of the entropy wave to those of the sound waves, as well as the dispersion equations for the waves involved.

In section 3, Lagrangian and Hamiltonian formulations of the equations were established for the lowest-order interaction case ($m = 1$ and $n = -1$) in which the wavelengths of the

backward and forward sound waves ℓ_1 and ℓ_3 are twice that of the entropy wave (ℓ_2) (Majda and Rosales [1] in fact restricted their attention solely to this case). The Lagrangian variational principle (equations (3.10) and (3.11)) was established by introducing velocity potentials U and V for the forward and backward sound wave velocity perturbations u and v and then expressing the equations in potential form. The other important point to note is the skew adjoint character of the matrix integral operator describing three-wave resonant interactions. An example of the Hamiltonian structure of the equations for a higher-order case in which the wavelengths of the backward sound wave (ℓ_1) and forward sound wave (ℓ_3) are related to the entropy wave of length ℓ_2 by the equations $\ell_1 = 4\ell_2$ and $\ell_3 = 2\ell_2$ was then considered.

In section 4, a study of the similarity solutions and conservation laws of the equations was carried out for the case of a periodic saw-tooth entropy wave profile in the fast phase variable θ. The analysis was restricted to cases where the backward and forward sound wave velocity perturbations u and v were independent of the large space variable x. Four conservation laws were established by exploiting the Lie point symmetries admitted by the potential form of the equations and by an application of Noether's theorem. Classical similarity solutions of the equations were derived using the Lie point symmetries. The Hamiltonians and canonical variables for two classes of similarity solutions obtained by Majda *et al* [9] corresponding to the travelling wave solutions and a periodic N-wave solutions with shocks were discussed.

Numerical examples of the similarity solutions of section 4, and more general solutions dependent on the large space variable x were used in section 5 to illustrate the interplay between nonlinear wave steepening and the dispersive three-wave resonant interactions. The travelling wave solutions considered by Majda *et al* [9] correspond to closed periodic orbits in the (u, v) phase plane obtained by plotting the contours of the Hamiltonian integral. These solutions can be considered as a special limit of more general similarity solutions. The more general solutions exhibit spiralling orbits about the origin in the appropriate (f, g) phase plane, and a more complex singularity structure involving critical points consisting of centres, saddles, nodes and spiral points. A generalization of the travelling wave solution of Majda *et al* [9] which depends on the large space variable x was studied. On the long space and timescales these solutions correspond to supersonic periodic travelling waves. The velocity amplitudes of the sound waves decrease monotonically to zero as the wave speed V_p approaches the sound speed c. As $\boldsymbol{V}_p \to \pm c\boldsymbol{e}_x$ the two pairs of saddles and centre critical points coalesce to form two cusp-like critical points which are hybrids between a centre and a saddle. In the subsonic regime $V_p < c$, no smooth, periodic travelling wave solutions with constant wave speed exist.

Hamiltonian equations in Fourier (p, t) space were derived in section 6, where p is the Fourier-space variable corresponding to the fast phase variable θ of the waves. The Hamiltonian in Fourier space was transformed to normal form (e.g. [20, 21]) in order to isolate the normal modes of the system. The characteristic frequencies in Fourier space are $\omega_p = |K_p|$, where K_p is the pth Fourier coefficient corresponding to the entropy wave kernel $K(\theta)$ occurring in the three-wave resonant interaction integrals.

Further aspects of three-wave resonant interactions of interest that deserve further attention consist of a more direct derivation of the Majda Rosales [1] equations using the Hamiltonian formulation of adiabatic, non-isentropic gas dynamics (e.g. [20]), and further analysis of the Hamiltonian Fourier space equations. Also of interest are related equations derived by Hunter *et al* [8] describing three-wave resonant interactions in adiabatic gas dynamics in two or more spatial dimensions, in which case the sound waves can be resonantly reflected by both the entropy wave and vorticity eigenmodes.

Acknowledgments

We acknowledge stimulating discussions with V E Zakharov, J K Hunter and C D Levermore. The work of GMW was supported in part by NASA grants NAG 1931 and NAGW 5055. AZ was supported in part by JPL contract 959377 with the Caltech. Jet Propulsion Lab. (Ulysses mission), and in part by NSF grant ATM 9520135 MB was supported in part by AFOSR under grant F49620 92J0054 GPZ was supported in part at the BRI by the NASA SPT programme under grant NAGW-2076, and in part by an NSF Young Investigator award ATM 935 7861.

Appendix

In this appendix we describe the periodic orbits of the Hamiltonian (5.1). From equation (5.1) the Hamiltonian contours are equivalent to the cubic equations:

$$v^3 - 3\frac{\lambda}{2}v - 3\tilde{H}_0 = 0 \qquad \tilde{H}_0 = H_0 - \frac{u^3}{3} + \frac{\lambda}{2}u^2. \tag{A1}$$

For the periodic orbits within EFBDE in figure 1, equations (A1) have three real roots for u and v given by the equations:

$$\begin{aligned} v_1 &= \lambda\cos\left(\frac{\theta}{3}\right) + \frac{\lambda}{2} \qquad v_2 = \lambda\cos\left(\frac{\theta+2\pi}{3}\right) + \frac{\lambda}{2} \qquad v_3 = \lambda\cos\left(\frac{\theta+4\pi}{3}\right) + \frac{\lambda}{2} \\ u_1 &= \lambda\cos\left(\frac{\phi}{3}\right) + \frac{\lambda}{2} \qquad u_2 = \lambda\cos\left(\frac{\phi+2\pi}{3}\right) + \frac{\lambda}{2} \qquad u_3 = \lambda\cos\left(\frac{\phi+4\pi}{3}\right) + \frac{\lambda}{2} \end{aligned} \tag{A2}$$

where

$$\cos\theta = 1 + \cos\theta_0 - \cos\phi \equiv 1 + 12\frac{\tilde{H}_0}{\lambda^3} \qquad \cos\theta_0 = 1 + 12\frac{H_0}{\lambda^3}. \tag{A3}$$

Note that $v_1 > v_3 > v_2$ and $u_1 > u_3 > u_2$. The periodic orbits inside EFBDE are described by u_2, u_3, v_2 and v_3, where $0 \leqslant \phi \leqslant \theta_0 < \pi$ and $0 \leqslant \theta \leqslant \theta_0$. The period T of the periodic orbits within EFBDE are given by

$$T = \oint \mathrm{d}\eta = 2\pi\frac{\mathrm{d}I}{\mathrm{d}H_0} \tag{A4}$$

where

$$I = \frac{1}{2\pi}\oint p_1\,\mathrm{d}q_1 \equiv -\frac{\lambda^4}{8\pi\alpha}\int_0^{\theta_0}\sin\left(\frac{\theta}{3}\right)\left[1+\cos\left(\frac{\theta}{3}\right)\right]\left[\cos\left(\frac{\phi}{3}\right)+\cos\left(\frac{2\phi}{3}\right)\right]\mathrm{d}\phi \tag{A5}$$

is the action (e.g. [17]). Equations (A4) and (A5) yield

$$T = \frac{\lambda}{\alpha}\int_0^{\theta_0}\frac{[\cos(\frac{1}{3}\phi)+\cos(\frac{2}{3}\phi)][\cos(\frac{1}{3}\theta)+\cos(\frac{2}{3}\theta)]}{\sin\theta}\,\mathrm{d}\phi. \tag{A6}$$

for the period of the orbits within EFBDE. For the critical contour ($H_0 = -\lambda^3/6$) $T = T_c$ and for the limiting orbit about $A(0,0)$ as $H_0 \to 0$ ($T \to T_0$) we have

$$T_c = \frac{\lambda}{\alpha}\left(3 + \frac{3^{\frac{1}{2}}\pi}{2}\right) \qquad T_0 = 2\pi\frac{\lambda}{\alpha}. \tag{A7}$$

Note that $T_c \leqslant T \leqslant T_0$ for the periodic orbits inside EFBDE.

References

[1] Majda A and Rosales R 1984 *Stud. Appl. Math.* **71** 149–79
[2] Almgren R F 1990 *Stud. Appl. Math.* **83** 159–81
[3] Joly J L, Metivier G and Rauch J 1993 *J. Funct. Anal.* **114** 106–231
[4] Grimshaw R 1988 *J. Fluid Mech.* **190** 357
[5] Cehelsky P and Rosales R 1986 *Stud. Appl. Math.* **74** 117–38
[6] Webb G M, Brio M, Zank G P and Story T R 1997 *J Plasma Phys.* **54** 1–46
[7] Anile A M, Hunter J K, Pantano P and Russo G 1993 *Ray Methods for Nonlinear Waves in Fluids and Plasmas* (Harlow: Longmans)
[8] Hunter J K, Majda A and Rosales R 1986 *Stud. Appl. Math.* **75** 187–226
[9] Majda A, Rosales R and Schonbeck M 1988 *Stud. Appl. Math.* **79** 205–62
[10] Pego R 1988 *Stud. Appl. Math.* **79** 263–70
[11] Hunter J K 1991 *Microlocal Analysis and Nonlinear Waves (IMA Volumes in Mathematics and it's Applications 30)* ed M Beals, R Melrose and J Rauch (New York: Springer) pp 83–112
[12] Magri F 1978 *J. Math. Phys.* **19** 1156
[13] Bluman G W and Kumei S 1989 *Symmetries and Differential Equations* (New York: Springer)
[14] Olver P J 1986 *Applications of Lie Groups to Differential Equations* (New York: Springer)
[15] Ince E L 1956 *Ordinary Differential Equations* (New York: Dover)
[16] Goursat E 1917 *A Course in Mathematical Analysis, Differential Equations* vol 2, part 2 (Boston, MA: Ginn.)
[17] Zaslavsky G M, Sagdeev R Z, Usikov D A and Chernikov A A 1991 *Weak Chaos and Quasi-regular Patterns* (Cambridge: Cambridge University Press)
[18] Lax P D 1973 *Hyperbolic Systems of Conservation Laws and the Mathematical Theory of Shock Waves (SIAM Regional Conf. Series in Appl. Math. No 11)*
[19] Chorin A J and Marsden J E 1979 *A Mathematical Introduction to Fluid Mechanics* (New York: Springer)
[20] Zakharov V E and Kusnetsov E A 1984 Hamiltonian formalism for systems of hydrodynamic type *Sov. Sci. Rev.* C **4** 167–220
[21] Zakharov V E, Musher S L and Rubenchik A M 1985 *Phys. Rep.* **129** 285–366